JOURNAL OF PETROLOGY | VOLUME 50 | NUMBER 3 | PAGES 427–449 | 2009 | doi:10.1093/petrology/egp006

Partial Melting of Mantle and Crustal Sources beneath South Karakorum, Pakistan: Implications for the Miocene Geodynamic Evolution of the India–Asia Convergence Zone

G. MAHÉO[1]*, J. BLICHERT-TOFT[1], C. PIN[2], S. GUILLOT[3] AND A. PÊCHER[3]

[1]UNIVERSITÉ DE LYON, F-69622, LYON, FRANCE UNIVERSITÉ LYON 1, VILLEURBANNE ENS, LYON CNRS, UMR 5570, LABORATOIRE DE SCIENCES DE LA TERRE, BAT GÉODE, 2 RUE DUBOIS, 69622 VILLEURVANNE, FRANCE

[2]LABORATOIRE DE GÉOLOGIE, CNRS-UMR 6524, UNIVERSITÉ BLAISE PASCAL, 5 RUE KESSLER, 63038 CLERMONT-FERRAND, FRANCE

[3]LABORATOIRE DE GÉODYNAMIQUE DES CHAÎNES ALPINES, CNRS-UMR 5025, OSUG, UNIVERSITÉ J. FOURIER, MAISON DES GÉOSCIENCES, B.P. 53, 38041 GRENOBLE, FRANCE

RECEIVED JUNE 29, 2005; ACCEPTED JANUARY 20, 2009
ADVANCE ACCESS PUBLICATION FEBRUARY 27, 2009

In south Karakorum, the western prolongation of southern Tibet, three distinct types of magmatic rocks were emplaced during the Neogene: (1) 22–24 Myr old lamprophyres, characterized by strong enrichment in large ion lithophile (LILE) and light rare earth elements (LREE), $^{87}Sr/^{86}Sr_{(i)} = 0{\cdot}7096$, $\varepsilon_{Nd(i)} = -7$, *and* $\varepsilon_{Hf} = -9$, *interpreted to reflect partial melting of a previously metasomatized spinel-lherzolite mantle source; (2) the 21–26 Myr old Baltoro high Ba–Sr granitoids, likewise strongly enriched in LILE and LREE, with* $^{87}Sr/^{86}Sr_{(i)} = 0{\cdot}7034$–$0{\cdot}7183$, $\varepsilon_{Nd(i)} = -6{\cdot}5$ *to* $-11{\cdot}0$, *and* $\varepsilon_{Hf} = -1{\cdot}8$ *to* $-8{\cdot}0$, *produced by partial melting of amphibole-bearing rocks in the lower crust, possibly the root of south Karakorum Cretaceous magmatic arc; (3) the 8–9 Myr old Hemasil syenite and its associated lamprophyre, also both enriched in incompatible elements but with isotopic compositions closer to those of depleted mantle* ($^{87}Sr/^{86}Sr_{(i)} = 0{\cdot}7043$–$0{\cdot}7055$, $\varepsilon_{Nd(i)} = +3{\cdot}5 - +4{\cdot}3$, *and* $\varepsilon_{Hf} = +10{\cdot}4 - +11{\cdot}2$). *The Hemasil syenite is interpreted as the product of partial melting of a time-integrated depleted spinel-lherzolite source that was enriched in K and LREE during a recent metasomatic event. We propose that the lamprophyres were formed during partial melting of the South Asian mantle previously metasomatized by fluids derived from the subducted Indian continental crust. This melting episode is interpreted to be related to a break-off event that occurred within the subducting Indian continental lithosphere. Intrusion of the resulting lamprophyric melts into the previously thickened south Karakorum crust caused partial melting of calc-alkaline igneous protoliths and generation of the Baltoro granitoids. Late-stage syenitic magmas were produced by low-degree partial melting during upwelling and adiabatic decompression of depleted mantle along the Shigar strike-slip fault.*

KEY WORDS: *India–Asia convergence zone; Karakorum; bimodal magmatism; slab break-off; heat advection*

INTRODUCTION

The evolution of collisional orogenic belts is associated with successive emplacement of a variety of magmatic rocks (Bonin, 1988). First, magmas related to partial melting of the metasomatized asthenospheric mantle wedge above a subduction zone are emplaced during oceanic and, possibly, subsequent continental subduction. At a

*Corresponding author. Telephone: +33 4 72 44 62 36.
E-mail: gmaheo@univ-lyon1.fr

later second stage, crustal melting may occur, mainly associated with crustal thickening and subsequent thermal re-equilibration following continent–continent collision. Finally, melting of the previous active continental margin lithosphere may take place in relationship with geodynamic processes that will be discussed below. This evolutionary sequence has been observed in a number of orogenic belts, such as those of Anatolia, Turkey (Harris *et al.*, 1994), the Austro-Italian Alps (Kagami *et al.*, 1991), the Oranides in Algeria (Hernandez *et al.*, 1987), the Betics of southern Spain (Venturelli *et al.*, 1984), and the Tibetan plateau (Coulon *et al.*, 1986; Miller *et al.*, 1999; Williams *et al.*, 2004). Most of the late-stage magmatic activity is interpreted to be related to partial melting of previously metasomatized spinel-facies lherzolite in the sub-continental lithospheric mantle (Kagami *et al.*, 1991; Turner *et al.*, 1996; Coulon *et al.*, 2002). In some cases (e.g. Anatolia and the Oranides), however, the latest magmatic stages have been interpreted to reflect partial melting of a depleted garnet-facies lherzolite source (Aldanmaz *et al.*, 2000; Coulon *et al.*, 2002).

Among the various regions worldwide where late orogenic magmatism has been observed, the Tibetan plateau is one of the most important. Here, igneous activity is found in two distinct provinces of the plateau, in north and south Tibet, without obvious spatial continuity. The north Tibetan magmatic rocks were emplaced from 45 Ma to the present (Arnaud *et al.*, 1992; Turner *et al.*, 1996; Guo *et al.*, 2006). They are mostly interpreted as related to the melting of enriched asthenospheric mantle, with some contribution from the metasomatically enriched continental lithosphere, as well as from the Tibetan crust (Guo *et al.*, 2006). In southern Tibet and in its western prolongation, the south Karokorum (Fig. 1), the magmatic rocks have been dated at between 8 and 25 Ma (Coulon *et al.*, 1986; Miller *et al.*, 1999; Williams *et al.*, 2001, 2004; Chung *et al.*, 2003; Ding *et al.*, 2003; Hou *et al.*, 2004; Nomade *et al.*, 2004) and exhibit a wide range of chemical and isotopic compositions. These magmatic rocks are located within a narrow, east–west-trending zone parallel to the Indus–Tsangpo Suture Zone (ITSZ, Fig. 1). In southern Tibet, the geochemical characteristics are widely interpreted in terms of melting of a previously metasomatized phlogopite-bearing spinel-facies lherzolite mantle source combined with variable degrees of crustal contamination (Coulon *et al.*, 1986; Turner *et al.*, 1996; Miller *et al.*, 1999; Williams *et al.*, 2001, 2004). Partial melting of the eclogitized lower part of the Asian continental crust also has been suggested (Chung *et al.*, 2003; Hou *et al.*, 2004; Qu *et al.*, 2004; Guo *et al.*, 2007).

Three main geodynamic processes have been considered to play a role in the south Tibetan Neogene magmatism: (1) continental subduction (Arnaud *et al.*, 1992; Ding *et al.*, 2003); (2) thinning of the lithospheric root beneath the Tibetan plateau by delamination (Houseman *et al.*, 1981; Turner *et al.*, 1996; Miller *et al.*, 1999; Williams *et al.*, 2001; Nomade *et al.*, 2004; Chung *et al.*, 2005; Guo *et al.*, 2007); (3) break-off of the subducting Indian continental lithospheric slab (Miller *et al.*, 1999; Mahéo *et al.*, 2002; Hou *et al.*, 2004; Williams *et al.*, 2004). However, partial melting can also result from thermal re-equilibration by radioactive heating of the thickened crust (e.g. Thompson & Connolly, 1995) or from shear heating along major strike-slip faults (e.g. Leloup *et al.*, 1999). Consequently, in a given area, broadly contemporaneous magmas can be produced by a variety of different processes.

In south Karakorum, a wide variety of Neogene magmatic rocks are observed. These include lamprophyres, high Sr–Ba granites, and syenites. Here, based on previously published and new major, trace, rare earth element (REE), and Sr, Nd, and Hf isotope data, we assess whether the Neogene magmatic evolution of south Karakorum as a whole can be explained within the framework of a single geodynamic model. We find that the generation of lamprophyre magmas is best explained by the break-off of the Indian continental lithosphere. In this scenario, the intrusion of mafic magmas into the previously thickened south Karakorum crust induced partial melting of granodiorites and diorites within the middle crust and the formation of peraluminous granites. The syenite parental magmas were produced later during mantle upwelling and adiabatic decompression controlled by the Shigar strike-slip fault.

GEOLOGICAL SETTING

The south Karakorum forms part of the pre-collisional south Asian continental margin, located to the west of, and separated from, southern Tibet by the Karakorum Fault (KF, Fig. 1). The eastern part of the south Karakorum basement corresponds to a Precambrian active continental margin (Rolland *et al.*, 2002*a*), whereas the western part is probably related to a Cambrian period of continental rifting (Le Fort *et al.*, 1994; Rolland *et al.*, 2002*a*). Both basement areas are covered by a thick Cambro-Ordovician sedimentary cover (Le Fort *et al.*, 1994; Rolland *et al.*, 2002*a*). Based on these characteristics, Rolland *et al.* (2002*a*) proposed that the south Karakorum is the westward propagation of the Lhasa block. The south Karakorum Precambrian to Cambrian basement is separated from the north Karakorum Permian to Jurassic sedimentary cover by the Early Ordovician Masherbrum volcanic complex (Rolland *et al.*, 2002*a*).

The south Karakorum Mesozoic to Cenozoic tectonic evolution is characterized by three major successive thermo-tectonic events. First, during the Early Cretaceous, as a result of the northward subduction of the

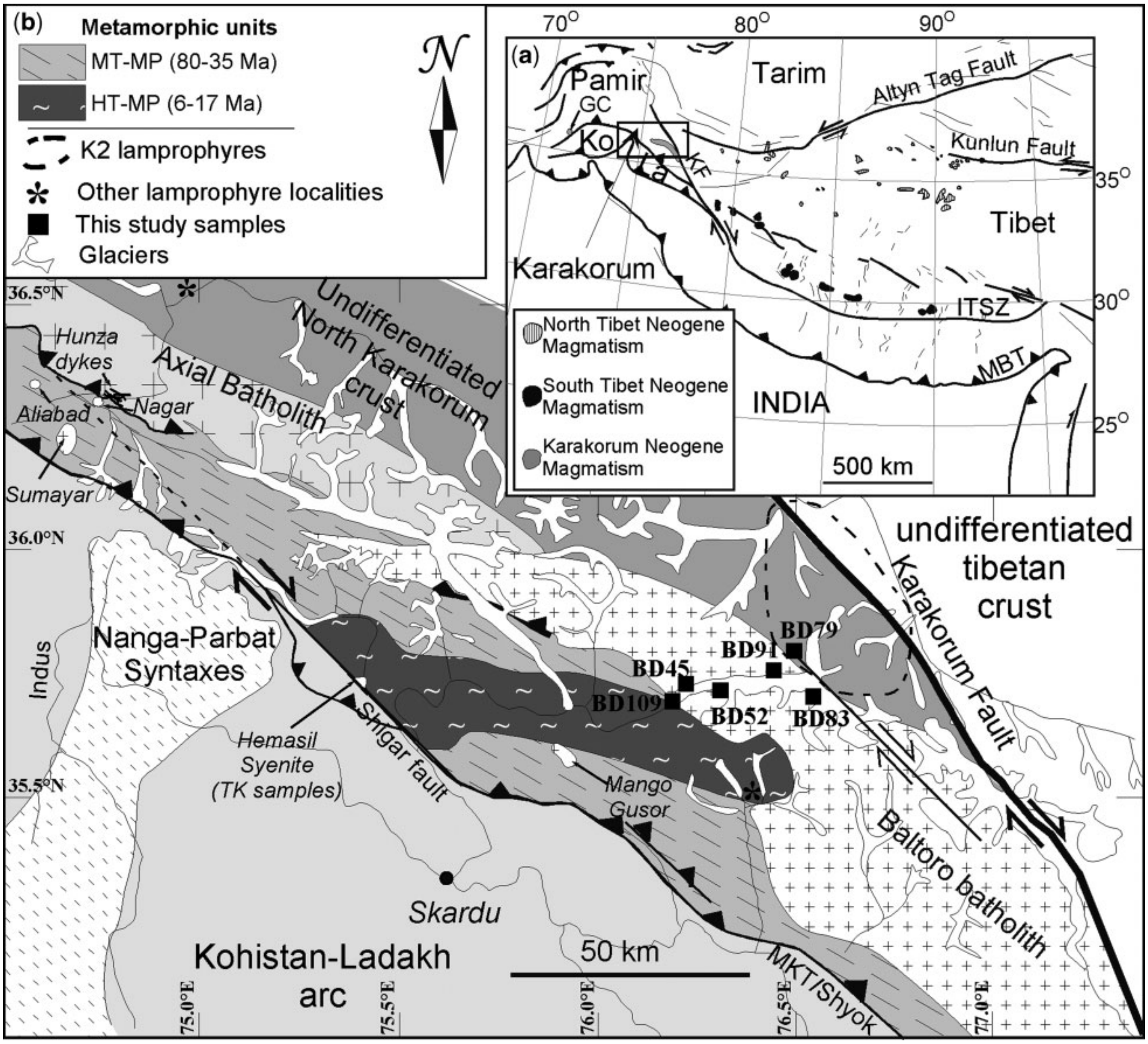

Fig. 1. (a) Location map of the late-orogenic magmatic rocks in the India–Asia convergence zone (After Arnaud *et al.*, 1992; Turner *et al.*, 1996; Chung *et al.*, 1998; Miller *et al.*, 1999; Ding *et al.*, 2003) and (b) geological map of south Karakorum (after Pêcher & Le Fort, 1999; Rolland *et al.*, 2001). South Karakorum lamprophyre and shoshonite locations after Pognante (1991), Searle *et al.* (1992) and Zanchi & Gaetani (1994). GC, Garam Chasma pluton; Ko, Kohistan; La, Ladakh; ITSZ, Indus–Tsangpo Suture Zone; MBT, Main Boundary Thrust; MKT, Main Karakorum Thrust; KF, Karakorum Fault.

Neo-Tethys oceanic lithosphere (Debon *et al.*, 1987; Crawford & Searle, 1992; Debon & Khan, 1996), calc-alkaline plutonic rocks were emplaced, forming the Axial Batholith (Fig. 1). During the mid-Cretaceous, continued subduction resulted in the opening of a back-arc basin separating the Karakorum margin from the Kohistan–Ladakh arc (Rolland *et al.*, 2000, 2002*b*). Collision of the Kohistan–Ladakh oceanic island arc and the Asian continental margin along the Shyok Suture Zone at ~75 Ma (Petterson & Windley, 1992) was followed by continent–continent collision with the Indian plate (Treloar *et al.*, 1989; Rowley, 1996). Stacking of southward-directed nappes was associated with the development of medium-temperature (MT)–medium-pressure (MP) metamorphism (Searle *et al.*, 1989; Lemmenicier *et al.*, 1996; Rolland *et al.*, 2001) and crustal melting, as suggested by the occurrence of numerous leucogranitic dykes (Hunza dykes; Fig. 1; Fraser *et al.*, 2001). Sub-alkaline felsic and mafic rocks were emplaced during this period, both in Karakorum (Batura complex; Debon *et al.*, 1987; Debon, 1995) and in NE Kohistan (Teru volcanics; Khan *et al.*, 2004). It has been proposed that these magmas were produced by partial melting of a depleted mantle source located above the Indian slab during continental subduction (Debon *et al.*, 1987; Debon, 1995; Khan *et al.*, 2004). The end of the nappe stacking event has not been precisely dated, but recent studies suggest an early Oligocene age (Fraser *et al.*, 2001; Rolland *et al.*, 2001). High-temperature (HT)–medium-pressure (MP) metamorphism took place during the Neogene, associated with the emplacement of late orogenic lamprophyres and granitoids (Bertrand *et al.*, 1988; Searle *et al.*, 1989; Lemennicier, 1996; Rolland *et al.*, 2001). Mahéo *et al.* (2004) proposed that subsequently the metamorphic rocks were partially exhumed by diapiric ascent within the lower and middle crust, followed by the uplift and erosion of southeastern Karakorum. In a previous study (Mahéo *et al.*, 2002), three groups of Neogene potassic igneous rocks were identified, the south Karakorum lamprophyres, the Baltoro batholith, and the Hemasil syenite.

The main post-crustal thickening magmatic unit is the Baltoro batholith (Fig. 1). This batholith is ~100 km long and 20 km wide, and is located in southeastern Karakorum, between the main Karakorum Thust (MKT) and the Karakorum Fault. The batholith is made of various granitoids constituting a suite between two end-members, which are (1) dark biotite granites rich in K-feldspar and containing plagioclase, quartz, titanite, magnetite, apatite, allanite and very rare amphibole and (2) leucogranites with some muscovite, plagioclase, K-feldspar, quartz, subordinate biotite and rare garnet. Based on U–Pb zircon ages, this batholith was emplaced between 26 and 21 Ma (Parrish & Tirrul, 1989; Schärer *et al.*, 1990). Other contemporaneous plutonic units include the Mango Gusar two-mica granite (dated at 26 Ma by U–Pb on zircon and allanite, Fraser *et al.*, 2001), also located in SE Karakorum, and the Garam Chasma leucogranite (dated at 24 Ma by U–Pb on monazite, xenotime, and uraninite, Hildebrand *et al.*, 1998) located in SW Karakorum, eastern Hindu Kush (see inset in Fig. 1). South of the Baltoro batholith, metasedimentary country-rocks are cross-cut by lamprophyre dykes (the south Karakorum or K2 lamprophyres; Rex *et al.*, 1988; Pognante, 1991; Searle *et al.*, 1992) dated at 22–24 Ma by K–Ar on biotite (Rex *et al.*, 1988). Other occurrences of lamprophyre veins have been reported east of the Mango Gusar granite, close to the western rim of the Baltoro batholith and north of the Axial Batholith (Fig. 1). Undeformed andesitic dykes also have been observed in central Karakorum, cross-cutting north Karakorum sediments (Gaetani *et al.*, 1996).

The youngest magmatic body in the area is the Hemasil syenite (Fig. 1), a 5 km diameter pluton, emplaced at 8–9 Ma along the Shigar Fault in southeastern Karakorum (Villa *et al.*, 1996). The 9·3 Ma Sumayar leucogranite (U–Pb on uraninite and monazite, Fraser *et al.*, 2001) located in south–central Karakorum (Fig. 1) is a contemporaneous pluton. Other post-crustal thickening granites have been observed, but their crystallization ages are still poorly constrained: the Nagar granite in south–central Karakorum with a K–Ar whole-rock age of 14·4 Ma (Fig. 1; Debon *et al.*, 1987) and the Aliabad granite with K–Ar muscovite and biotite ages between 4·5 and 6·8 Ma (Fig. 1; Le Fort *et al.*, 1983).

ANALYTICAL METHODS

Selected trace elements (Rb, Sr, Y, Zr, Nb and Pb) for five samples of granitoids from the Baltoro batholith (BD45, BD52, BD83, BD91, BD109) and one south Karakorum lamprophyre (BD79, see Fig. 1 for location), all collected by F. Debon and J.-M. Bertrand, as well as four Hemasil syenite samples (TK506, TK836, TK837, TK841) and one Hemasil lamprophyre (TK838), collected by P. Le Fort, Y. Lemennicier and A. Pêcher, were determined by wavelength-dispersive X-ray fluorescence spectrometry (XRF) at the University of Lyon. Analytical uncertainties range from 1 to 2% for major elements and from 10 to 15% for trace elements.

The concentrations of some additional trace elements (Ba, Hf, Ta, and REE) of samples TK506 and BD79 were analyzed by inductively coupled plasma mass spectrometry (ICP-MS) at Ecole Normale Supérieure de Lyon (ENS Lyon). Analytical uncertainties are less than 5%. All data are listed in Table 1.

Sr and Nd isotopic compositions were measured by thermal ionization mass spectrometry in Clermont-Ferrand, using an upgraded VG 54E instrument operated in dynamic triple collection mode, with correction for mass fractionation by normalization to $^{86}Sr/^{88}Sr = 0{\cdot}1194$ and $^{146}Nd/^{144}Nd = 0{\cdot}7219$, respectively. Prior to mass spectrometric analyses, Sr and Nd were isolated by tandem extraction chromatography using Sr Spec, TRU Spec, and Ln Spec materials (Eichrom S.A., Paris), following separation procedures described in detail by Pin *et al.* (1995) and Pin & Santos Zalduegui (1997) for sample dissolution of granitoid rocks and final isolation of Nd. During the period of analysis, the SRM 987 Sr carbonate standard from NIST gave a mean value of $^{87}Sr/^{86}Sr = 0{\cdot}710242$ ($\sigma = 0{\cdot}000015$, $n = 13$), and the Nd standard JNdi-1 from the Geological Survey of Japan (Tanaka *et al.*, 1996) gave a mean value of $^{143}Nd/^{144}Nd = 0{\cdot}512111$ ($\sigma = 0{\cdot}000007$, $n = 7$). Sr and Nd total procedural blanks were better than 1 ng and 0·5 ng, respectively. We measured the Sr and Nd isotopic compositions of four Hemasil syenites (TK506, TK837, TK839, TK841), one Hemasil lamprophyre (TK838), five Baltoro batholith granites (BD45, BD52, BD83, BD91, BD109) and the lamprophyre located north

Table 1: Selected whole-rock analyses of Hemasil and Baltoro samples from south Karakorum

Location:	Hemasil	Hemasil	Hemasil	Hemasil	Hemasil	Hemasil	Hemasil	Hemasil	Baltoro	Baltoro	Baltoro	Baltoro	Baltoro	Baltoro	K2	K2	K2	K2
Sample:	TK506	TK835	TK836	TK837	TK839	TK841	TK845	TK838	BD45	BD52	BD83	BD91	BD109	BD79	R11	1880	1943	1882
Type:	Syenite	Syenite	Syenite	Syenite	Syenite	Syenite	Syenite	Lamp.	Dark gran.	Dark gran.	Dark gran.	Leuco-gran.	Dark gran.	Lamp.	Lamp.	Lamp.	Lamp.	Lamp.
SiO_2	58·27	54·42	53·57	58·26	57·24	59·78	56·49	35·48	69·38	71·79	72·4	73·79	66·75	57·55	52·9	50·46	57·57	62·03
TiO_2	0·63	0·45	0·66	0·50	1·00	0·5	0·34	2·75	0·36	0·31	0·29	0·18	0·49	0·71	1·62	0·75	0·81	0·7
Al_2O_3	19·31	20·09	21·17	18·45	20·21	19·79	20·77	17·73	16·03	14·68	14·92	13·6	16·12	16·35	10·3	11·66	15·71	15·35
Fe_2O_3	3·08	4·95	4·25	4·13	3·41	2·74	2·39	15·96	2·49	1·82	1·63	1·2	2·73	6·22	6·9	7·22	7·72	6·39
MnO	0·3	0·24	0·23	0·16	0·15	0·22	0·54	0·51	0·06	0·03	0·04	0·03	0·04	0·09	0·12	0·11	0·11	0·08
MgO	0·85	0·25	0·76	2·19	0·55	0·54	0·35	5·61	0·67	0·41	0·27	0·28	1·04	2·54	11·1	6·64	3·87	2·41
CaO	3·00	3·38	5·85	1·14	4·12	2·35	3·36	13·71	2·24	1·84	1·33	0·59	2·82	4·93	6	6·7	5·04	4·99
Na_2O	5·25	2·03	3·04	4·03	3·38	6·13	4·61	1·18	4·46	4·09	3·92	3·3	4·21	2·77	1·1	1·33	2·12	2·58
K_2O	7·25	10·64	7·42	8·62	8·77	7·03	7·74	2·41	3·29	3·55	4·5	5·3	3·74	4·31	7·95	3·95	4·9	3·04
P_2O_5	0·15	0·09	0·21	0·29	0·16	0·13	0·07	1·47	0·09	0·00	0·00	0·00	0·16	0·36	1·7	0·72	0·77	0·24
LOI	1·63	3·10	1·05	0·81	0·98	0·57	2·42	1·51	0·55	0·36	0·42	0·40	0·47	4·01		10·83	2·51	2·49
Total	99·64	99·78	99·08	98·21	99·97	98·58	99·72	98·32	99·62	98·88	99·72	98·67	98·57	99·84	99·69	100·37	101·13	100·30
Ba	**158**	314	3108	1046	364	191	89	2434	1168	1106	971	495	889	**872**	3679·5	2346·0	1935·0	832·0
Rb	**134**	201	**162**	**188**	107	**126**	202	**54**	**169**	**117**	253	**236**	**131**	**190**	358·4	169·0	176·0	87·0
Sr	**649**	1021	**4319**	**580**	1774	**445**	846	**4543**	**647**	**581**	406	**220**	**1076**	**525**	1221·4	708·0	1154·0	389·0
Ta	**2·21**	0·27	0·75	0·47	0·81	0·41	0·64	0·12						**1·49**				
Th	**13·2**	9·1	2·6	1·3	2·7	6·6	19·2	1·1	20·2	7·8	26·7	1·4	20·6	**17·2**	78·1	21	24	17
Zr	**594**	162	**70**	**68**	61	**155**	380	**44**	**194**	**168**		**100**	**217**	**194**	692	226	276	226
Nb	**10·7**	5·9	**7·3**	**6·5**	5·8	**7·0**	12·4	**1·3**	**17·0**	**7·1**		**16·3**	**13·8**	**12·5**	46·3	17	22	15
Y	**39·8**	21·0	**23·4**	**12·1**	35·5	**23·5**	29·4	**26·1**	**11·9**	**6·5**	10·2	**15·9**	**9·4**	**24·3**	34·3	26·2	33·9	29·6
Hf	**0·5**	3·3	2·0	1·7	1·8	3·7	9·9	1·6						**3·7**				
U	**1·4**	4·6	0·9	0·1	0·7	1·6	5·4	0·1	6·3	10·4	8·8	7·6	8·1	**3·9**	10·5			
Pb	**31·2**	16·9	**17·1**	**8·4**	13·8	**17·7**	66·3	**14·4**	**34·5**	**34·5**		**85·5**	**48·7**	**20·3**	105·9			
La	**73·6**	31·7	29·4	10·2	26·4	31·4	49·6	34·4	47·0	40·1	38·3	22·4	69·3	**70·7**	137·0	44·3	59·4	41·5
Ce	**136·9**	60·9	72·1	21·8	71·8	61·1	84·3	81·3	81·7	65·9	67·0	40·3	128·8	**144·9**	275·0	88·7	115·7	82·4
Pr	**15·8**	6·7	10·2	2·8	11·3	6·9	8·0	11·7						**16·5**				
Nd	**57·3**	24·3	45·7	12·3	53·8	25·9	25·5	57·6	35·3	27·5	28·8	18·3	51·7	**64·2**	121·0	36·3	49·0	33·1
Sm	**10·4**	4·3	9·9	3·0	12·6	4·9	4·1	13·0	6·0	4·7	4·9	4·3	8·1	**11·0**	22·0	7·3	9·8	6·7
Eu	**1·9**	1·2	3·4	0·8	3·8	1·1	0·6	4·1	0·9	0·8	0·8	0·6	1·8	**2·1**	4·5	1·7	2·4	1·5
Gd	**7·4**	3·5	7·3	2·4	9·3	3·9	3·5	9·7	4·4	3·3	3·5	3·7	5·7	**8·1**		5·7	7·5	5·8
Tb	**1·0**	0·6	1·1	0·4	1·4	0·6	0·6	1·3						**1·0**	1·4			
Dy	**6·0**	3·2	6·2	2·2	7·5	3·5	3·7	7·0	2·5	1·5	2·1	2·9	2·6	**4·7**		4·2	5·3	4·6
Ho	**1·2**	0·8	1·2	0·4	1·5	0·8	1·0	1·3						**0·7**				
Er	**3·7**	2·1	2·8	1·1	3·2	2·1	3·1	2·8	1·1	0·8	1·0	1·3	1·3	**2·0**		2·1	2·6	2·5
Yb	**3·6**	2·2	2·3	1·1	2·4	2·5	4·3	2·0	0·9	0·6	0·7	1·2	0·9	**1·4**	1·9	1·9	2·4	2·3
Lu	**0·5**	0·3	0·3	0·2	0·3	0·4	0·7	0·3	0·2	0·1	0·1	0·2	0·2	**0·2**	0·2	0·4	0·5	0·4

Bold font, this study; normal font, Hemasil from Lemmenicier (1996), Baltoro granites from Debon *et al*. (1986) and Debon (personal communication), K2 lamprophyres from Pognante (1991) and Searle *et al*. (1992). Major elements are in oxide wt %, other elements are in ppm. Lamp., lamprophyre; Gran., granite; Leucogran., leucogranite.

of the Baltoro batholith (BD79). The data are given in Table 2. We further re-analyzed the Sr and Nd isotopic compositions of sample TK841, previously measured by Lemmenicier (1996). The two sets of measurements are in good agreement, thus allowing our new data to be compared directly with those obtained on the Hemasil pluton by Lemmenicier (1996).

Sm and Nd concentrations of the Hemasil samples are from Lemmenicier (1996), except for sample TK506 (this study). Sm and Nd concentrations for the Baltoro samples are from Debon *et al.* (1986) and F. Debon (personal communication), except for sample BD79 (this study).

We also measured the Hf isotopic compositions of three Hemasil syenite samples (TK506, TK836, TK837),

Table 2: Nd, Sr and Hf isotopic compositions of lamprophyres, syenites, and granites from south Karakorum

		$^{143}Nd/^{144}Nd$	$^{147}Sm/^{144}Nd$	$^{143}Nd/^{144}Nd_{(i)}$	$\varepsilon_{Nd(i)}$	$^{87}Sr/^{86}Sr$	$^{87}Rb/^{86}Sr$	$^{87}Sr/^{86}Sr_{(i)}$	$^{176}Hf/^{177}Hf$	$\varepsilon_{Hf(present\ day)}$
Hemasil										
Syenite	TK839	0·512857 ± 6*	0·1415	0·512849	+4·3	0·704353 ± 13*	0·17	0·704331	0·283092 ± 10†	+11·3
Syenite	TK835	0·512810 ± 9*	0·1075	0·512804	+3·5	0·705140 ± 10*	0·56	0·705068	0·283065 ± 23†	+10·4
Syenite	TK845	0·512816 ± 6*	0·0975	0·512810	+3·6	0·705621 ± 12*	0·68	0·705534	0·283098 ± 19†	+11·1
Syenite	TK841	0·512820 ± 6*	0·1141	0·512813	+3·6	0·705603 ± 16*	0·74	0·705503		
Syenite	TK841	0·512835 ± 6	0·1141	0·512828	+3·9	0·705638 ± 11	0·74	0·705543	0·283091 ± 11†	+11·3
Syenite	TK506	0·512833 ± 7	0·1097	0·512827	+3·9	0·705549 ± 11	0·43	0·705493	0·283117 ± 10	+12·2
Syenite	TK836	0·512836 ± 6	0·1307	0·512828	+3·9	0·704328 ± 09	0·15	0·704308	0·283104 ± 06	+11·7
Syenite	TK837	0·512828 ± 7	0·1479	0·512819	+3·8	0·705254 ± 14	0·86	0·705143		
Lamp.	TK838	0·512818 ± 6	0·1369	0·512810	+3·6	0·704294 ± 11	0·05	0·704287	0·283108 ± 07	+11·9
Baltoro										
Granite	BD45	0·512287 ± 7	0·1034	0·512270	−6·5	0·708821 ± 12	0·75	0·708552	0·282692 ± 07	−2·8
Granite	BD52	0·512176 ± 7	0·1020	0·512159	−8·7	0·707733 ± 13	0·64	0·707503	0·282720 ± 06	−1·8
Granite	BD83	0·512188 ± 8	0·1020	0·512171	−8·5	0·709704 ± 16	1·77	0·709073	0·282621 ± 07	−5·3
Granite	BD91	0·512067 ± 8	0·1431	0·512044	−11·0	0·712984 ± 10	3·15	0·711864	0·282592 ± 06	−6·4
Granite	BD109	0·512251 ± 8	0·1037	0·512234	−7·3	0·708887 ± 12	0·59	0·708674	0·282545 ± 07	−8·0
Lamp.	BD79	0·512254 ± 8	0·1033	0·512238	−7·2	0·709876 ± 09	0·74	0·709644	0·282508 ± 05	−9·3

*From Lemmenicier (1996).
†From Maheo *et al*. (2002).
Uncertainties reported on Nd, Sr, and Hf measured isotope ratios are in-run $2\sigma/\sqrt{n}$ analytical errors in last decimal places, where n is the number of measured isotopic ratios. Sr and Nd initial isotope compositions were corrected for radiogenic ingrowth using $^{147}Sm/^{144}Nd$ and $^{87}Rb/^{86}Sr$ ratios calculated from the trace element data given in Table 1 and emplacement ages of 9 Ma for the Hemasil samples, 25 Ma for the Baltoro granites, and 22 Ma for the Baltoro lamprophyre. ε_{Nd} and ε_{Hf} values correspond to the fractional deviation in parts per 10^4 from the contemporaneous value of a chondritic (Bulk Earth) reservoir with present-day $^{143}Nd/^{144}Nd = 0{\cdot}512638$ and $^{147}Sm/^{144}Nd = 0{\cdot}1966$ (Jacobsen & Wasserburg, 1980) and $^{176}Hf/^{177}Hf = 0{\cdot}282772$ (Blichert-Toft & Albarède, 1997), respectively. As precise Lu and Hf concentrations are not available for the Baltoro granites, the present-day ε_{Hf} values only are reported.

one Hemasil lamprophyre (TK838), five Baltoro granite samples (BD45, BD52, BD83, BD91, BD109) and one Baltoro lamprophyre (BD79). These data supplement those previously published by Mahéo *et al.* (2002) on four Hemasil syenite samples (TK835, TK839, TK841, TK845). The data are listed in Table 2. The separation of Hf for isotopic analysis was carried out at ENS Lyon following the protocols outlined by Blichert-Toft *et al.* (1997) and Blichert-Toft (2001). Hf isotopic analysis was carried out by multicollector (MC)-ICP-MS using a Plasma 54 system at ENS Lyon following the procedure of Blichert-Toft *et al.* (1997). Mass fractionation was corrected relative to $^{179}Hf/^{177}Hf = 0{\cdot}7325$, and the JMC-475 Hf standard, which was run systematically after every two samples to monitor machine performance, gave $0{\cdot}282160 \pm 10$ (2σ) during the course of this study. Hf total procedural blanks were better than 25 pg. We did not measure the Lu/Hf ratios, but given the young ages of the samples investigated here, the age correction is negligible.

ISOTOPIC AND GEOCHEMICAL CHARACTERISTICS

South Karakorum lamprophyres

The petrographic characteristics of the lamprophyres are relatively variable, characterized by an association of phlogopite, plagioclase, apatite and alkali feldspar with occasional hornblende, augite, quartz and accessory titanite and zircon (Rex *et al.*, 1988; Pognante, 1991; Searle *et al.*, 1992). Secondary white mica, chlorite and calcite have also been observed (Pognante, 1991). The sample analyzed in this study, BD79, contains phlogopite, hornblende, plagioclase, alkali feldspar and apatite.

All the lamprophyres are intermediate rocks belonging to the alkaline suite (Fig. 2). Data from Pognante (1991) and Searle *et al.* (1992) plot within the ultrapotassic and shoshonitic field in a K_2O vs Na_2O diagram (Fig. 2). The lamprophyres exhibit a wide range of Mg-number values (from 0·64 to 0·30) and SiO_2 contents (from 50·5 to 62·0 wt %). The petrography of the more differentiated

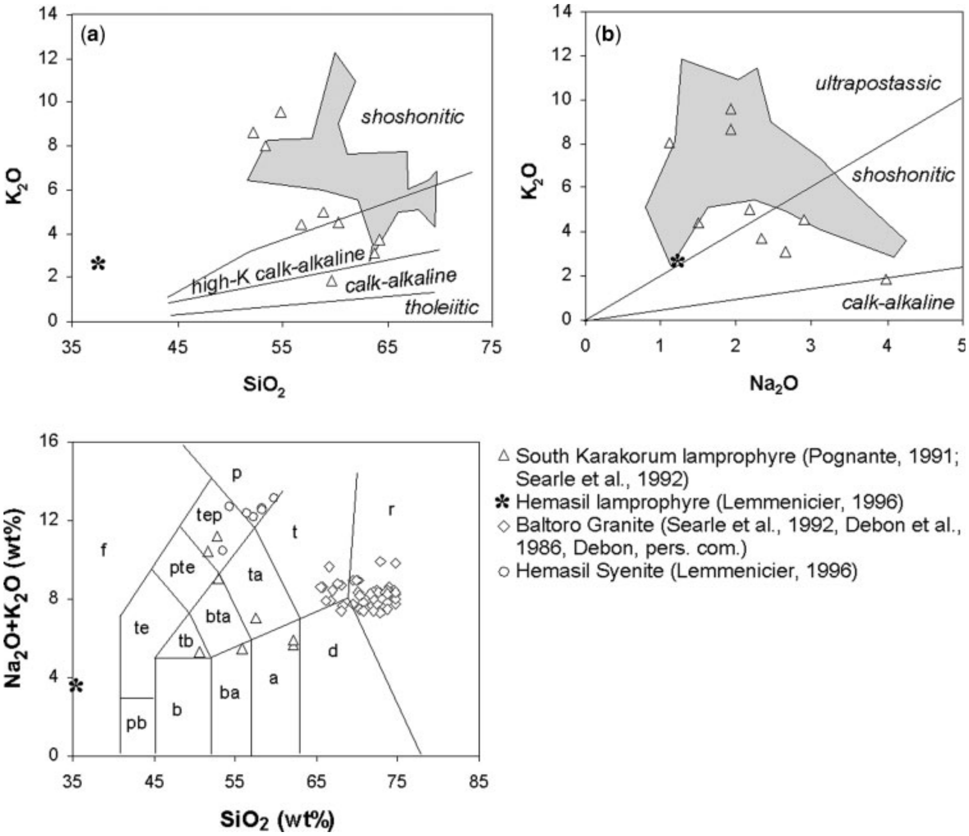

Fig. 2. (a) K_2O vs SiO_2 (wt %) and (b) K_2O vs Na_2O (wt %) for south Karakorum and Hemasil lamprophyres. Shaded field represents the Neogene southern Tibetan ultrapotassic and potassic volcanic rocks (Miller *et al.*, 1999; Williams *et al.*, 2001, 2004; Ding *et al.*, 2003; Nomade *et al.*, 2004). (c) Total alkalis vs SiO_2 diagram of Le Maitre *et al.* (1989). a, andesite; b, basalt; ba, basaltic andesite; bta, basaltic trachyandesite; d, dacite; f, foidite; t, trachyte; ta, trachyandesite; tb, trachybasalt; te, tephrite; tep, tephriphonolite; pte, phonotephrite; p, phonolite; pb, picrobasalt; r, rhyolite.

samples (lowest Mg-number) is characterized by the presence of hornblende and occasional augite. Clinopyroxene is not observed in the more primitive samples (Mg-number > 0·5). The most primitive samples (Mg-number > 0·6) are characterized by relatively low Al_2O_3, CaO, and Na_2O contents (10–11 wt %, 6·1–7·4 wt %, and 1·1–1·9 wt %, respectively) and very high abundances of K_2O (8·0– 8·7 wt %). Volatile contents are usually significant [loss on ignition (LOI) up 10·8 wt %]. The most elevated values (>6 wt %) were determined in two samples with clear petrographic evidence of severe alteration (presence of calcite, white micas and chlorite). All the south Karakorum lamprophyres have primitive mantle-normalized multi-element patterns (Fig. 3a) characterized by strong enrichment in large ion lithophile elements (LILE) and light REE (LREE) relative to high field strength elements (HFSE) and heavy REE (HREE) (Pognante, 1991; Searle *et al.*, 1992).

The lamprophyre analyzed in this study (BD79) has a radiogenic $^{87}Sr/^{86}Sr_{(i)}$ (0·7096) and unradiogenic $\varepsilon_{Nd(i)}$ (−7·2) isotope signature, albeit less extreme than those of the lamprophyres analysed by Searle *et al.* (1992) from south Karakorum ($^{87}Sr/^{86}Sr_{(i)} = 0·7160–0·7200$ and $\varepsilon_{Nd(i)}$ ∼−12; Fig. 4). The isotopic compositions of the lamprophyres analyzed by Searle *et al.* (1992) resemble those of the contemporaneous ultrapotassic and potassic rocks from southern Tibet (Turner *et al.*, 1996; Miller *et al.*, 1999; Williams *et al.*, 2001, 2004; Nomade *et al.*, 2004).

The lamprophyre BD79 has a relatively low ε_{Hf} of −9·3. It plots on the mantle array within the field of intracontinental basalts interpreted to be associated with lithospheric melting (Fig. 5; Beard & Johnson, 1993; Johnson & Beard, 1993; Barry *et al.*, 2003).

Baltoro batholith

As discussed above, the Baltoro batholith consists of various granitoids constituting a continuous suite between two end-members, one of which is a dark biotite granite, rich in poikilitic K-feldspar and containing plagioclase, quartz, titanite, magnetite, apatite, allanite and very rare amphibole, whereas the other is a leucogranite with some muscovite, plagioclase, K-feldspar, quartz, subordinate

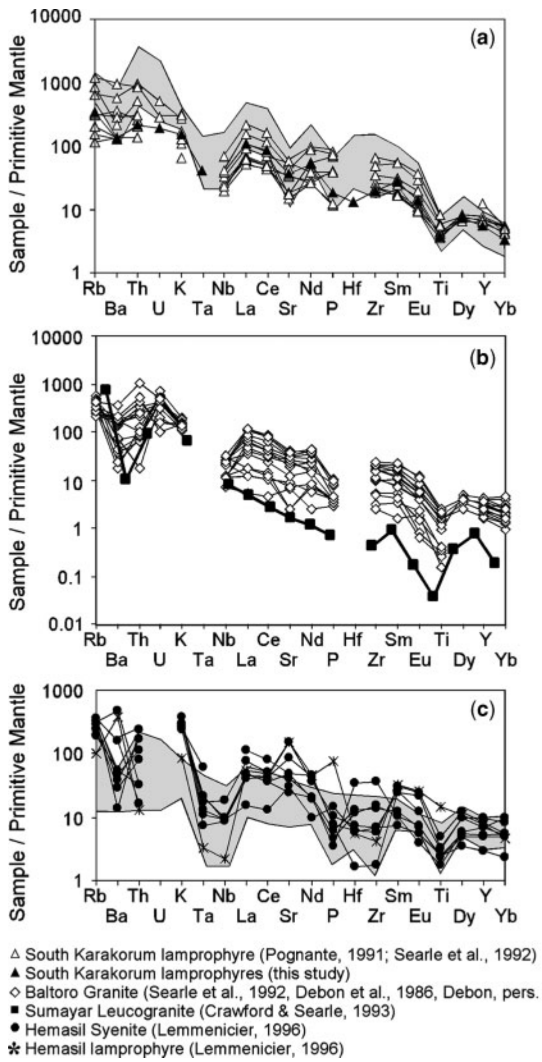

Fig. 3. Primitive mantle-normalized multi-element diagrams for (a) south Karakorum lamprophyres, (b) Baltoro granites, and (c) Hemasil syenites and associated lamprophyre. Primitive mantle normalization values from McDonough & Sun (1995). In (a), the light grey shaded field represents the Neogene southern Tibetan ultrapotassic and potassic volcanic rocks (Miller *et al.*, 1999; Williams *et al.*, 2001, 2004; Ding *et al.*, 2003; Nomade *et al.*, 2004). In (c), the light grey shaded field represents the Teru volcanics (Khan *et al.*, 2004).

biotite and rare garnet. The samples studied here are representative of this suite. BD109 and 45 are dark biotite porphyritic granites with poikilitic K-feldspar, plagioclase and some apatite, magnetite and titanite. BD52 and 83 are intermediate biotite granites with poikilitic K-feldspar, plagioclase and minor apatite. BD91 is a leucogranite, also with poikilitic K-feldspar, abundant plagioclase, muscovite and trace amounts of biotite. BD45 is an aplitic granite with both muscovite and biotite, perthitic K-feldspar, abundant plagioclase and some magnetite. The Baltoro granitoids are characterized by relatively high SiO_2, Na_2O, Al_2O_3, and K_2O contents (65·5–74·8 wt %, 3·3–6·8 wt %, 13·6–17·3 wt %, and 3·0–6·0 wt %, respectively) and low TiO_2, MgO, FeO_T, and CaO (<0·8 wt %, <1·3 wt %, <3·0 wt %, and <3·0 wt %, respectively). The SiO_2 contents increase from dark biotite granite to leucogranite as TiO_2, Al_2O_3, FeO_T, MgO, CaO, and P_2O_5 contents decrease. The dark biotite granites are magnesian alkali–calcic to magnesian calc-alkaline, whereas the leucogranites are ferroan calc-alkaline (Fig. 6) according to the classification of Frost *et al.* (2001). In a primitive mantle-normalized multi-element diagram (Fig. 3b), all the granitoids are characterized by a strong enrichment in LILE and LREE relative to HFSE and HREE (Searle *et al.*, 1992) with Ba, Sr, Th, Zr and LREE higher for dark biotite granites than for leucogranite. Based on their high Ba and Sr concentrations and low Y, HREE and Nb contents the dark biotite granites are reminiscent of the high Ba–Sr granites defined by Tarney & Jones (1994).

The samples analyzed in this study show a wide range of initial Nd and Sr isotopic compositions, as do the samples analyzed by Schärer *et al.* (1990) and Searle *et al.* (1992; Fig. 4). $^{87}Sr/^{86}Sr_{(i)}$ ranges from 0·7034 to 0·7183 and $\varepsilon_{Nd(i)}$ from −6·5 to −11·0. The dark biotite granites and leucogranites have similar isotopic compositions. The isotopic compositions of all the Baltoro samples are additionally similar to those of the magmatic rocks emplaced in south Karakorum during the period of Cretaceous active margin activity (Fig. 4; Crawford & Searle, 1992). ε_{Hf} for the Baltoro granitoids varies between −2·8 and −8·0. In an ε_{Hf} vs ε_{Nd} diagram, most of the samples plot above the mantle array, outside the field defined by 98% of mid-ocean ridge basalt (MORB) and ocean island basalt (OIB) (Fig. 5) and close to the field of pelagic sediments and ferromanganese nodules (Godfrey *et al.*, 1997; Albarède *et al.*, 1998; Vervoort *et al.*, 1999), the latter of which have been interpreted to record the isotopic properties of fine-grained material settling in the deep ocean (Blichert-Toft *et al.*, 1999).

Hemasil syenite

The 9 Ma Hemasil syenite and associated lamprophyre belong to the last magmatic event recorded in south Karakorum. Three main parageneses occur among the syenite samples: K-feldspar + plagioclase + biotite ± epidote (TK506, 836, 837), K-feldspar + plagioclase + amphibole ± biotite ± epidote (TK838, 839, 841) and K-feldspar + plagioclase + biotite + muscovite + calcite (TK835, 845). Minor zircon, apatite and titanite are also present in all lithologies (Lemennicier, 1996). The lamprophyre (TK838) is composed of amphibole, epidote, biotite, K-feldspar and plagioclase with minor titanite and chlorite (Lemennicier, 1996). All the syenite samples have moderate SiO_2 contents (53·6–59·8 wt %), relatively low TiO_2,

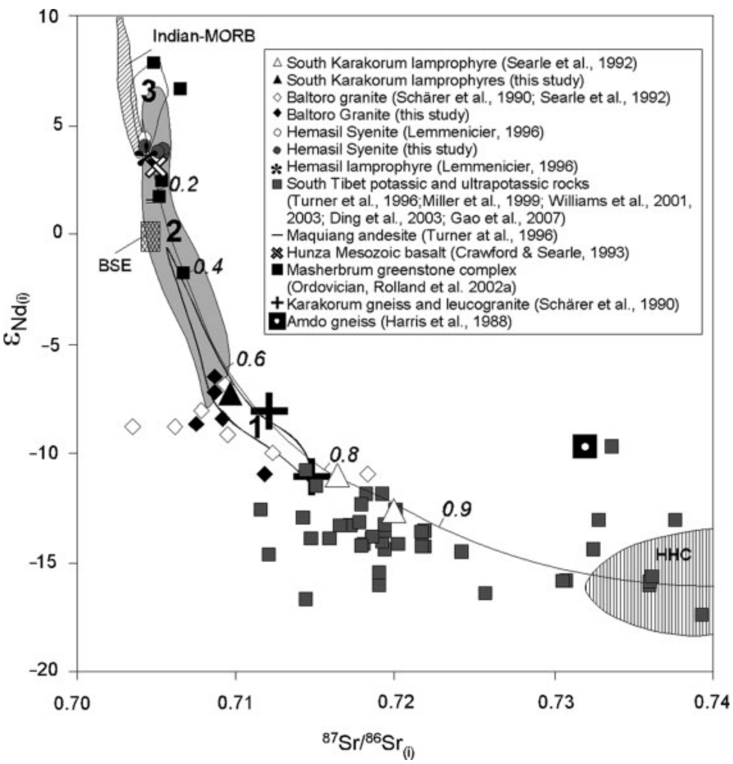

Fig. 4. Initial $^{87}Sr/^{86}Sr$ vs initial ε_{Nd} for the south Karakorum and southern Tibetan Neogene magmatic rocks. The data for the Baltoro granite were recalculated at 25 Ma, those for the Baltoro lamprophyres at 22 Ma, the Hemasil syenite and lamprophyre at 9 Ma, the Hunza Mesozoic rocks at 95 Ma, and the Karakorum gneiss and leucogranite, Amdo gneisses and Masherbrum Greenstone complex at 20 Ma. The data for the South Tibetan potassic and ultrapotassic rocks are from Turner *et al.* (1996), Miller *et al.* (1999), Williams *et al.* (2001, 2004), Ding *et al.* (2003) and Gao *et al.* (2007). Field 1, south Karakorum Cretaceous calc-alkaline active margin recalculated at 95 Ma (Crawford & Searle, 1993). Field 2, Kohistan–Ladakh and south Tibet Cretaceous arc magmatic rocks (Allègre & Othman, 1980; Harris *et al.*, 1988; Petterson *et al.*, 1993; Khan *et al.*, 1997, 2004; Miller *et al.*, 2000; Rolland *et al.*, 2000, 2002*b*). Field 3, Kohistan–Ladakh Cretaceous back-arc basalts (Khan *et al.*, 1997; Rolland *et al.*, 2000, 2002*b*). Indian MORB field is from Mahoney *et al.* (1998). High Himalaya Crystalline (HHC) field is from Guillot (1993) and Guillot & Le Fort (1995). Bulk Silicate Earth (BSE) from Zindler & Hart (1986). The mixing line is a simple mass-balance calculation between an HHC leucogranite ($^{87}Sr/^{86}Sr = 0{\cdot}7417$, Sr 50 ppm, $\varepsilon_{Nd} = -16{\cdot}0$, Nd 11·6 ppm; Guillot, 1993) and a Teru volcanic rock ($^{87}Sr/^{86}Sr = 0{\cdot}7040$, Sr 455 ppm, $\varepsilon_{Nd} = +5{\cdot}4$, Nd 15 ppm; Khan *et al.*, 2004).

MgO, and FeO_t contents (0·3–1·0 wt %, 0·3–2·2 wt %, and 2·2–4·6 wt %, respectively), and very high Al_2O_3 and K_2O contents (19·3–21·2 wt % and 7·0–10·6 wt %, respectively). In a primitive mantle-normalized multi-element diagram (Fig. 3c), both the syenite samples and the cross-cutting lamprophyre are characterized by strong enrichment in LILE and LREE relative to HFSE and HREE (Lemennicier, 1996; Mahéo *et al.*, 2002). However, several patterns can be distinguished. The most primitive sample ($MgO = 2{\cdot}2$ wt %), a K-feldspar + plagioclase + biotite syenite, has a relatively smooth pattern characterized by strong LILE enrichment but only slightly negative Nb and Ti anomalies and no Zr and Hf anomalies. In comparison, other more differentiated ($MgO < 0{\cdot}9$ wt %) samples have similar LILE enrichment but stronger negative Nb, Zr, Hf and Ti anomalies with the exception of three samples with positive Zr and Hf anomalies, which are clearly related to the presence of abundant zircon. Moreover, the most differentiated sample ($MgO = 0{\cdot}35$ wt %), a K-feldspar + plagioclase + biotite + muscovite + calcite syenite, shows slight enrichment in HREE relative to MREE. The development of pronounced negative HFSE anomalies and HREE enrichment with differentiation can be explained by early crystallization of biotite, as documented in thin section (Lemennicier, 1996), followed by amphibole. Amphibole crystallization will produce residual liquids enriched in LILE and LREE and relatively depleted in HFSE, middle REE (MREE) and HREE. Rocks crystallizing from such a liquid will have primitive mantle-normalized multi-element patterns characterized by marked negative HFSE anomalies and in some cases enrichment in HREE as observed for most of the Hemasil syenite samples. The Hemasil lamprophyre primitive mantle-normalized multi-element pattern also is characterized by strong LILE and LREE enrichment and relative depletion in Nb, Zr, Hf and HREE. Such a pattern likewise is compatible with a residual liquid left after amphibole removal.

The Hemasil syenite samples have broadly homogeneous Sr and Nd isotopic compositions, ranging from 0·7043 to 0·7055 for initial $^{87}Sr/^{86}Sr$ and from $+3{\cdot}5$ to $+4{\cdot}3$ for initial ε_{Nd} (Fig. 4). The associated lamprophyre has a similar isotopic composition ($^{87}Sr/^{86}Sr_{(i)} = 0{\cdot}7043$ and $\varepsilon_{Nd(i)} = +3{\cdot}6$). Thus far, such positive ε_{Nd} values have not been reported for other Neogene magmatic rocks from the India–Asia convergence zone. The Neogene magmatic rocks showing the most depleted isotope signatures are the 10–15 Ma Maquiang andesites occurring near Lhasa in southern Tibet (Coulon *et al.*, 1986) with initial $^{87}Sr/^{86}Sr$ of 0·7048–0·7049 and initial ε_{Nd} between $+1{\cdot}3$ and $+1{\cdot}5$ (Fig. 4; Turner *et al.*, 1996). Isotopic compositions similar to those of the Hemasil syenite have also been observed in the most primitive Cretaceous and Paleocene tholeiitic to calc-alkaline rocks in the Gangdese batholith and in the 65–40 Ma Linzizong volcanic rocks, both from southern Tibet, as well as in the Chilas gabbronorite and the Teru volcanic rocks of the Kohistan–Ladakh arc (Fig. 4; Allègre & Othman, 1980; Harris *et al.*, 1988; Petterson *et al.*, 1993; Khan *et al.*, 1997, 2004; Miller *et al.*, 2000; Jagoutz *et al.*, 2006; Mo *et al.*, 2007, 2008). In south Karakorum, equivalent calc-alkaline rocks are found in the Cretaceous Axial Batholith (Crawford & Searle, 1992), where a basalt from the Hunza area has slightly more enriched isotope characteristics than the Hemasil syenite (initial $^{87}Sr/^{86}Sr = 0{\cdot}7050$ and initial $\varepsilon_{Nd} = +2{\cdot}8$; Fig. 4; Crawford & Searle, 1992). These isotopic compositions are also close to the least depleted Indian MORB (Mahoney *et al.*, 1998) and Kohistan–Ladakh back-arc basalts (Khan *et al.*, 1997; Rolland *et al.*, 2000, 2002*b*).

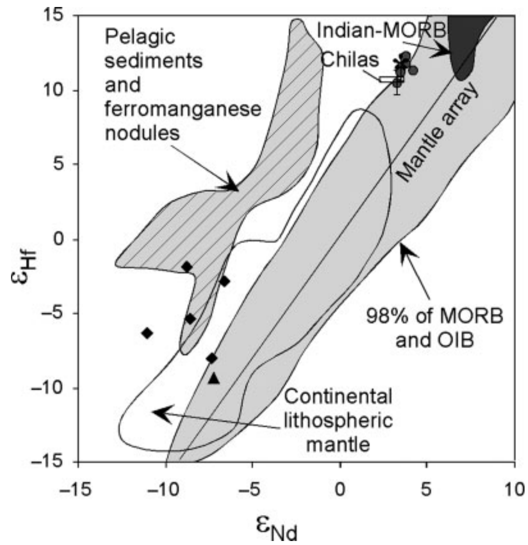

Fig. 5. ε_{Nd} vs ε_{Hf} for the Hemasil syenite and lamprophyre, the Baltoro granites, and one Baltoro lamprophyre (BD79). Same symbols as in Fig. 4. Mantle array based on published data (references too numerous to be cited here) and J. Blichert-Toft (unpublished data) Hf and Nd isotope data for ~2500 samples of OIB and MORB. Indian MORB field is from Nowell *et al.* (1998). Continental lithospheric mantle field is from Beard & Johnson (1993; Rio Grande Rift), Johnson & Beard (1993; NW Colorado), and Barry *et al.* (2003; Mongolia). The field for oceanic sediments (pelagic sediments and ferromanganese nodules) is from Godfrey *et al.* (1997), Albarède *et al.* (1998) and Vervoort *et al.* (1999). The Nd and Hf isotopic compositions for the Chilas complex are from Khan *et al.* (1997) and Schaltegger *et al.* (2002), respectively. Error bars are smaller than symbols, except for ε_{Hf} values of TK835 and 845. Symbols as in Fig. 2.

All the Hemasil samples have relatively homogeneous, fairly radiogenic Hf isotopic compositions (from $+10{\cdot}4$ to $+12{\cdot}2$; Fig. 5). Such values are comparable with those of the 85 Ma Chilas gabbronorites from the south Kohistan arc and the 50 Ma meta-gabbros from the north Kohistan arc (Schaltegger *et al.*, 2002; Heuberger *et al.*, 2007). They have been related to melting of fragments of old metasomatically enriched Asian continental lithosphere trapped beneath the Kohistan arc (Schaltegger *et al.*, 2002; Heuberger *et al.*, 2007). These isotopic compositions are

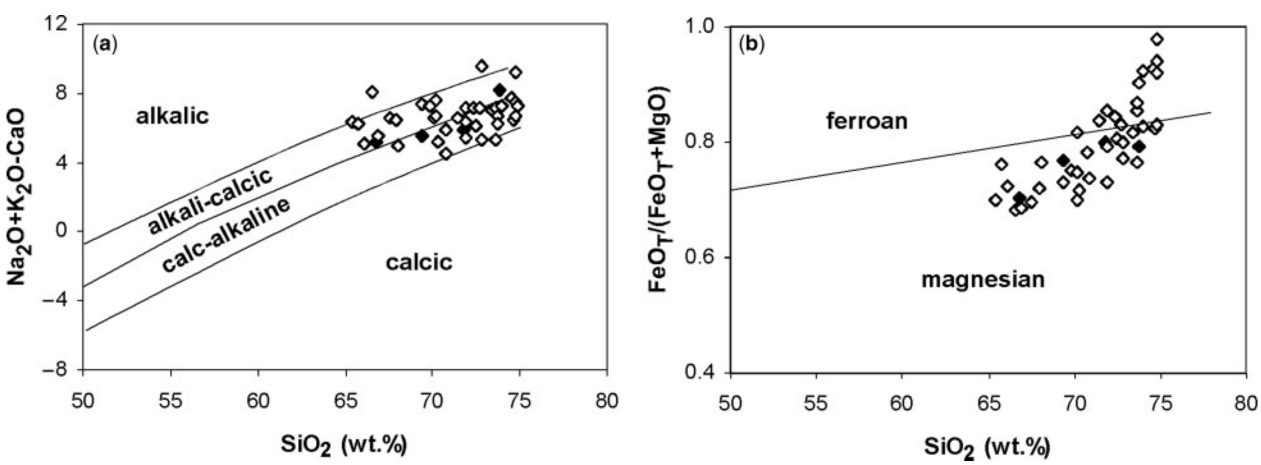

Fig. 6. Baltoro granitoid classification (after Frost *et al.*, 2001): (a) $Na_2O + K_2O - CaO$ vs SiO_2; (b) $FeO_T/(FeO_T + MgO)$ vs SiO_2. Open diamonds, Debon *et al.* (1986), Searle *et al.* (1992) and F. Debon (personal communication); filled diamonds, this study.

also close to those of the least depleted Indian Ocean MORB (Nowell *et al.*, 1998). However, as observed for the Baltoro samples, in an ε_{Hf} vs ε_{Nd} diagram, the Hemasil samples plot at the extreme end of the field defined by 98% of MORB and OIB (Fig. 5).

INFERRED SOURCES OF THE SOUTH KARAKORUM NEOGENE MAGMAS

South Karakorum lamprophyres

The south Karakorum lamprophyres exhibit chemical and isotopic heterogeneity that can be explained either by heterogeneous sources and/or open-system behaviour during intra-crustal evolution of the magmas. Based on their high concentrations of incompatible elements, relative enrichment in LILE and LREE, and Sr–Nd isotopic compositions, all the lamprophyres have been interpreted as the products of partial melting of a previously metasomatized source in the Asian lithospheric mantle (Pognante, 1991; Searle *et al.*, 1992; Mahéo *et al.*, 2002). This hypothesis is compatible with the Hf isotopic composition of BD79 ($\varepsilon_{Hf} = -9{\cdot}3$), which plots within the field interpreted to be representative of the continental lithosphere isotopic composition (Fig. 5; Beard & Johnson, 1993; Johnson & Beard, 1993; Barry *et al.*, 2003). A similar source was also proposed for the contemporaneous ultrapotassic and potassic magmatic rocks of southern Tibet (Miller *et al.*, 1999; Williams *et al.*, 2001, 2004; Ding *et al.*, 2003; Nomade *et al.*, 2004). Mahéo *et al.* (2002) and Ding *et al.* (2003) showed that on an initial $^{87}Sr/^{86}Sr$ vs ε_{Nd} diagram (Fig. 4), the south Karakorum lamprophyres and the southern Tibetan ultrapotassic and potassic magmatic rocks plot on a mixing trend between an end-member isotopically similar to the most primitive Cretaceous magmatic rocks from Karakorum, the Kohistan–Ladakh arc and the Gangdese batholith and an end-member similar to the Higher Himalayan leucogranites (HHL) or their inferred source, the Higher Himalayan Crystalline (HHC; Guillot & Le Fort, 1995). The Himalayan leucogranites are interpreted as the products of partial melting of Proterozoic metasedimentary rocks from the Indian continental margin (Guillot & Le Fort, 1995), whereas the Cretaceous calc-alkaline magmatism has been interpreted to reflect melting of a supra-subduction zone lithospheric and asthenospheric mantle wedge during the northward subduction of the Neo-Tethys ocean floor beneath the Asian active margin (Coulon *et al.*, 1986; Debon *et al.*, 1987; Crawford & Searle, 1992; Miller *et al.*, 2000). It should be noted that, because of potential crustal assimilation, the isotopic composition of the more isotopically depleted samples can only be considered as the closest approximation of the true isotopic composition of the Asian supra-subduction zone mantle at that time (Crawford & Searle, 1992; Miller *et al.*, 2000). This implies that the observed ε_{Nd} and $^{87}Sr/^{86}Sr$ signature are respectively minimum and maximum values of the composition of the Asian supra-subduction zone mantle, which in turn means that the estimated involvement of these end-members, as inferred from mixing calculations such as those of Fig. 4, will be underestimated.

To assess the role of contamination of mantle-derived magmas by the Karakorum crust it is necessary to consider the various units constituting this area. Three main rock-types can be distinguished: the volumetrically dominant Cretaceous calc-alkaline diorites and granodiorites, the metamorphic rocks, and the Precambrian to Cambro-Ordovician basement. However, the occurrence of other lithologies present at greater depth cannot be ruled out. The only isotopic data from the Karakorum Precambrian to Cambro-Ordovician crust are from the Masherbrum greenstones (Rolland *et al.*, 2002*a*). These exhibit ε_{Nd} and $^{87}Sr/^{86}Sr$ values, recalculated at 20 Ma, ranging from $-1{\cdot}9$ to 7·8 and from 0·7052 to 0·7067, respectively. Another estimate of the isotopic composition of the Karakorum basement is based on the data from the Lhasa block basement, interpreted as the eastward prolongation of the Karakorum (Rolland *et al.*, 2002*a*); specifically, the Amdo orthogneiss characterized by ε_{Nd} values at 20 Ma ranging from $-9{\cdot}6$ to $-11{\cdot}3$ and $^{87}Sr/^{86}Sr$ at 20 Ma between 0·7319 and 0·7443. The range of initial $^{87}Sr/^{86}Sr$ and ε_{Nd} values from the Cretaceous calc-alkaline rocks most probably reflects mixing processes between mafic magmas generated in the Asian supra-subduction zone mantle and the pre-Cretaceous Karakorum crust. The isotopic composition of the Karakorum gneisses is poorly constrained. Schärer *et al.* (1990) analysed a biotite gneiss and an associated granite giving ε_{Nd} and $^{87}Sr/^{86}Sr$ at 20 Ma of $-11{\cdot}2$ to $-8{\cdot}1$ and 0·7148–0·7121, respectively. When all these estimates of the isotopic composition of the various units forming the south Karakorum crust are plotted together with the south Karakorum lamprophyres (Fig. 4) it appears that although contamination of the lamprophyre parental magma by the Karakorum crust cannot be ruled out, it cannot explain the observed isotopic trend.

The observed trend for the lamprophyres on the initial $^{87}Sr/^{86}Sr$ vs ε_{Nd} plot could represent mixing between the supra-subduction zone Asian lithospheric and asthenospheric mantle wedge and Indian metasediments, with some possible involvement of the Karakorum crust. The Indian metasediment signature could reflect either a direct and major contribution (60–85% based on Fig. 4) of partial melt of metasedimentary protoliths, or alternatively, a mantle source reservoir that underwent an earlier metasomatic event related to a hydrous melt derived from these metasediments. For a given SiO_2

content (55–65 wt %), the lamprophyres have LILE concentrations and volatile contents significantly higher than the Cretaceous magmatic rocks produced by partial melting of the Asian supra-subduction mantle (Ba < 800 ppm; Sr < 510 ppm; LOI < 2 wt %; Crawford & Searle, 1992). The Indian metasediments and leucogranites also have significantly lower incompatible element concentrations than the lamprophyres (Ba < 600 ppm, Sr < 200 ppm, Deniel *et al.*, 1987; Inger & Harris, 1993; Guillot & Le Fort, 1995; Visona & Lombardo, 2002). Consequently, involvement of 60–85% of metasedimentary melts derived from the Indian slab may result in significantly lower lithophile element concentrations than observed. The trend toward the isotopic composition of the HHC, along with the enrichment in lithophile elements, implies that the mantle source of the lamprophyres was metasomatized by hydrous melts with a continental crust-like signature, largely derived from continental sediments, released from the subducting Indian continental margin. Such contamination has been demonstrated for the 55–45 Ma Asian upper mantle wedge by Guillot *et al.* (2001) and Hattori & Guillot (2007). This mantle was metasomatized by hydrous fluids derived from subducting clastic sediments of the Indian passive continental margin, resulting in the occurrence of high $^{87}Sr/^{86}Sr$ (0·70673–0·72997; Hattori & Guillot, 2007) and ε_{Nd} as low as –20 (Guillot *et al.*, 2001). A similar interpretation has been proposed for the southern Tibetan potassic and ultrapotassic rocks (Ding *et al.*, 2003; Gao *et al.*, 2007) and is reinforced by Fig. 4, in which the south Karakorum lamprophyres and the southern Tibetan potassic and ultrapotassic rocks plot along the same mixing line. However, Gao *et al.* (2007) recently proposed that the low Sr/Nd (3–10) and Ba/La (9–21), and high Th/Ce (0·3–1·0) and Th/Sm (3–7) ratios, as well as the HFSE and Th enrichment (Th 112–232 ppm, Nb 34–80 ppm, Ta 1·9–4·5 ppm, Zr 340–1100 ppm) observed in 25 Ma lamproites from south–central Tibet imply the involvement of 2–10% of sediment-derived melts in the magma source. Compared with these samples, for a given MgO content, only the two Karakorum lamprophyres described by Searle *et al.* (1992) present similar characteristics; in particular, a distinct enrichment in HFSE relative to the Cretaceous magmatic rocks produced by partial melting of the Asian supra-subduction mantle. Thus, for these two samples, involvement of sediment-derived melts seems likely but cannot exceed 3% according to the modelling of Gao *et al.* (2007). In conclusion, the magma source of the Karakorum lamprophyres is proposed to be the Asian supra-subduction zone mantle wedge contaminated by aqueous fluids and melts derived from sediments and released from the subducting Indian passive continental margin. Admittedly, the possible existence of a supra-subduction zone Asian lithospheric and asthenospheric mantle wedge with a heterogeneous isotopic composition resulting from various metasomatic events having occurred at different times cannot be ruled out. Nevertheless, the good fit of the data with the calculated mixing line in Fig. 4 suggests that the potential metasomatic events involved broadly similar fluids most probably derived from continental sediments and probably released from the subducting Indian continental margin. Finally, the similarity in isotopic compositions (Fig. 4), normalized trace element patterns (Fig. 3) and major element compositions (Fig. 2) between the south Karakorum lamprophyre and the southern Tibetan potassic and ultrapotassic rocks also suggests a similar source for these contemporaneous magmatic rocks.

Some of the south Karakorum lamprophyres are relatively primitive (Mg-number > 0·6). Therefore, their trace element and isotopic characteristics may be used to make inferences about the nature of their mantle source. These primitive lamprophyres are characterized by relatively high HREE and Y contents (1·9 ppm < Yb < 2·2 ppm and 0·2 ppm < Lu < 0·3 ppm, 9–14 times the chondritic values, and 34 ppm < Y < 55 ppm). Moreover, as Mg-number decreases, Y content decreases and HREE do not show any significant variation, suggesting that the primitive magmas also have high HREE and Y contents. Such characteristics suggest that there was no residual garnet in the source. These data are more compatible either with melting at shallow depths (<85 km) in the spinel stability field, or with total consumption of garnet during partial melting. Nevertheless, Miller *et al.* (1999) and Ding *et al.* (2003) pointed out that the La/Yb ratio (43·7–73·4) of the southern Tibetan ultrapotassic rocks is elevated and may be related to the extraction of a very small fraction of melt from a garnet-bearing source. However, detailed studies and geochemical modelling by Williams *et al.* (2004) have shown that such comparatively high La/Yb ratios could also be obtained by partial melting of a phlogopite- and amphibole-bearing mantle in the spinel-lherzolite facies.

Baltoro batholith

As discussed above, although all the Baltoro batholith samples show similar primitive mantle-normalized multi-element patterns (Fig. 3b), they present a wide range of Sr and Nd isotopic compositions (Fig. 4), implying that their parental magmas were extracted from sources with broadly similar chemistry and mineralogy, but distinct isotopic compositions, and/or experienced different petrogenetic evolutionary histories (e.g. variable degrees of crustal contamination).

Based on their high SiO_2 (65·5–74·8 wt %) and low MgO (<1·3 wt %) contents, the granitoids can be related either to extensive differentiation (with various degrees of crustal assimilation) of mantle-derived parental magmas, or to partial melting of crustal rocks.

The less differentiated, dark biotite granites are characterized by the presence of abundant K-feldspar, titanite, magnetite and very rare amphibole. Muscovite and garnet are observed only in the more differentiated leucogranites. These mineralogical characteristics suggest derivation from a more mafic precursor, either by extensive differentiation of a mantle-derived magma, or by partial melting of a basaltic or dioritic source. The only less differentiated and contemporaneous outcropping magmas are the lamprophyres, which have isotopic compositions close to those of the granitoids (Fig. 4). However, another potential source is provided by the calc-alkaline rocks from the south Karakorum Cretaceous active margin, which are isotopically similar to the Baltoro granitoids (Fig. 4). Inferences drawn about the mineralogical composition of the source of the batholith may help discriminate between these two hypotheses. The Baltoro granitoids are all characterized by high contents of Al_2O_3 (>15 wt % for SiO_2 < 70 wt %), Sr and Ba (>100 ppm and >400 ppm, respectively, for 70 wt % < SiO_2 < 74 wt %) and low Rb/Sr and K/Sr ratios (0·1–3·9 and 80–315, respectively). Such features are suggestive of melting of a plagioclase-bearing source in the presence of residual amphibole (Petford & Atherton, 1996). Moreover, the most primitive Baltoro granitoids (SiO_2 65–70 wt %) have relatively high $(La/Yb)_N$ (50–71), high Sr/Y (51–80), low Y and Yb contents (10–13 ppm and 0·7–0·9 ppm, respectively), and $(Er/Yb)_N$ >1. These characteristics are indicative of either refractory garnet in their source, or extraction of garnet from the melt by fractional crystallization. In Sr/Y vs Y and La/Yb vs Yb plots, the Baltoro granitoids define two groups (Fig. 7). The first group (with Sr/Y and La/Yb >20) corresponds to the less silicic samples (SiO_2 < 73 wt %) and plots within the field of adakites, whereas the second group (with Sr/Y and La/Yb <20) includes the most differentiated leucogranites (SiO_2 > 73 wt %) and plots within the field of common andesites–dacites–rhyolites. This difference is most probably related to fractional crystallization with progressive extraction of plagioclase, as is also suggested by strongly negative Eu anomalies in the most differentiated leucogranites. However, the fact that the less differentiated samples display adakitic affinities and that this signature decreases with differentiation supports the presence of residual garnet in the magma source. Therefore, the chemical characteristics of the Baltoro granitoids are indicative of melting in the presence of residual garnet followed by fractional crystallization. Altogether, the presence of both residual amphibole and garnet in the source favours the origin of the Baltoro granitoids by partial melting of a metabasaltic or metadioritic protolith. Such source material could occur in the deep-seated zones of the Cretaceous south Karakorum active margin, whose calc-alkaline rocks have the same isotopic signatures as the Baltoro granitoids. Also, the Cretaceous south Karakorum active margin calc-alkaline rocks and the Baltoro granitoids have similar T_{DM} Nd model ages (750–1500 Ma and 1000–1200 Ma, respectively). Only sample BD91 is significantly different with a Nd T_{DM} of 2000 Ma. However, this sample has the highest initial $^{87}Sr/^{86}Sr$ (0·71186) and lowest initial ε_{Nd} (−11), suggesting that massive crustal contamination occurred during its petrogenesis. Crustal contamination is also documented by the presence of old zircon cores (700–1750 Ma; Parrish & Tirrul, 1989; Schärer *et al.*, 1990). The incorporation into the parental magma of old

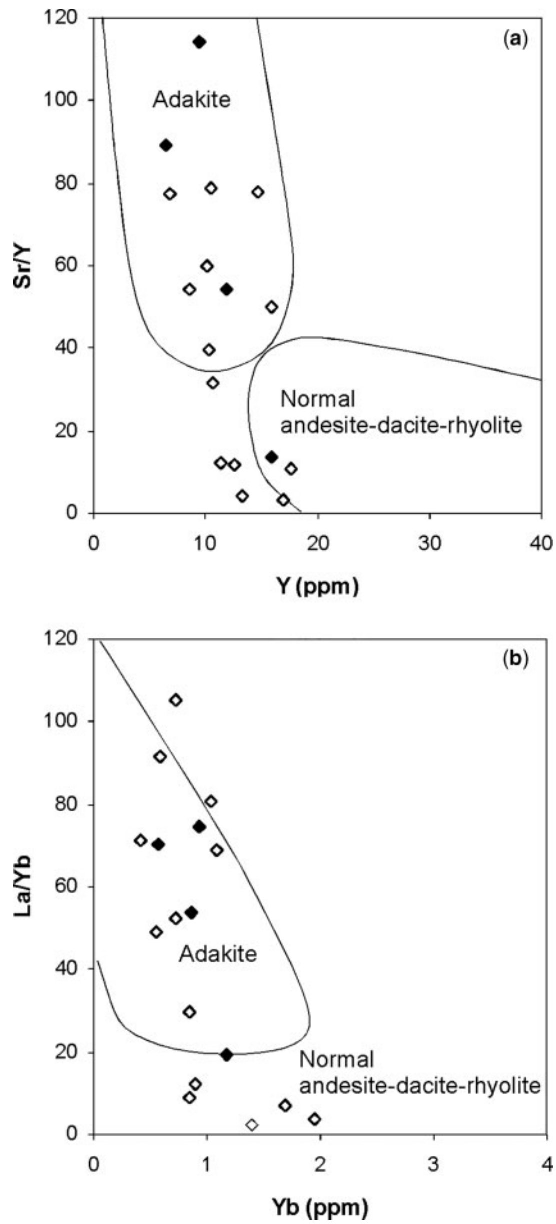

Fig. 7. (a) Sr/Y vs Y and (b) La/Yb vs Yb for the Baltoro granites. The high Sr/Y and La/Yb ratios together with the low Y and Yb contents are indicative of the presence of residual garnet in the source of the granites. Fields of adakite and normal andesites–dacites–rhyolites from Castillo *et al.* (1999). Same symbols as in Fig. 6.

inherited zircons from metasediments is further suggested by the observed scatter of whole-rock isotopic compositions between sedimentary and mantle fields in the ε_{Hf} vs ε_{Nd} diagram (Fig. 5). In southern Tibet, contemporaneous calc-alkaline rocks have been associated with partial melting of eclogite or garnet amphibolite located in the southern Tibetan lower crust (Chung *et al.*, 2003; Hou *et al.*, 2004; Guo *et al.*, 2007).

Numerous other peraluminous granitoids have been observed in south Karakorum. Their emplacement ages range from ~50 Ma for the early set of Hunza dykes to 9·3 Ma for the Sumayar Pluton (Fraser *et al.*, 2001). All of them have been interpreted in terms of partial melting of metapelitic sources. According to Crawford & Searle (1993), the formation of the parental magmas of the Hunza dykes, emplaced as two pulses between 50 and 35 Ma (Fraser *et al.*, 2001), was controlled by biotite breakdown. However, the close similarity between the Baltoro Granitoids and the Hunza dykes (high Ba and Sr, low Y and HREE) pointed out by Crawford & Searle (1993) suggests a similar origin, from relatively mafic protoliths. Therefore, we propose that both units are related to remelting of the roots of the south Karakorum Cretaceous magmatic arc. Leucogranites, such as the Garam Chasma Leucogranite located in the Indu Kush and emplaced contemporaneously with the Baltoro batholith (Zafar *et al.*, 2000, 2001) and the 9·3 Ma Sumayar pluton (Crawford & Searle, 1993), are significantly different from the Baltoro granitoids in that they contain, for a given SiO_2 content, much higher Y and Rb, and less Ba, Sr and REE and have high Rb/Sr ratios (Fig. 3). These characteristics are all more consistent with partial melting of metapelitic sources (Crawford & Searle, 1993; Zafar *et al.*, 2000, 2001).

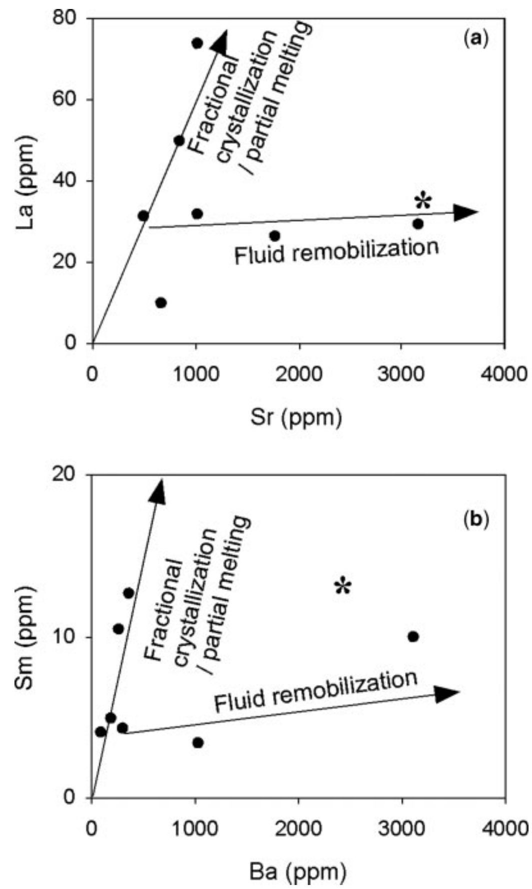

Fig. 8. La vs Sr (a) and Sm vs Ba (b) for the Hemasil syenites and the associated lamprophyre. The relationships observed in these plots allow for the identification of compositional variations related to fractional crystallization and remobilization by hydrothermal fluids (see text). Same symbols as in Fig. 4.

Hemasil syenite

The youngest magmatic unit of the south Karakorum, the Hemasil syenite and associated lamprophyre, has a fairly homogeneous Sr, Nd, and Hf isotopic composition suggesting a common origin. The Hemasil syenite and lamprophyre are characterized by high concentrations of incompatible elements. Primitive mantle-normalized multi-element diagrams (Fig. 3c) display enrichment in LILE (Ba, K, Rb, Sr) relative to REE and some HFSE (Ta, Nb). The HFSE define negative anomalies relative to REE. The LILE enrichment could have been produced by several different processes. For instance, as these elements are highly mobile in aqueous fluids, they could have been enriched by sub-solidus interaction with hydrothermal fluids. Alternatively, the observed enrichment could reflect either crustal contamination or earlier metasomatism of their mantle source, or both. Any secondary mobility of LILE as a result of post-magmatic alteration or weathering (e.g. Sr, Ba) can be evaluated by plotting their concentrations against those of other LILE or of immobile elements, such as La (Fig. 8a and b). Two trends are observed. The samples with the lowest (but still elevated relative to HFSE) LILE contents define a linear trend, which can be explained by fractional crystallization or partial melting. In contrast, the samples with the highest LILE concentrations are significantly shifted away from the fractional crystallization–partial melting trend. This shift is suggestive of secondary LILE remobilization, probably during late-stage, post-igneous interaction with hydrothermal fluids. To test the possibility of enrichment by crustal contamination, the LILE contents have been plotted against $^{87}Sr/^{86}Sr$ only using samples that define a crystallization–partial melting trend in the previous plot (Fig. 9). On the one hand, the Ba vs $^{87}Sr/^{86}Sr$ plot (Fig. 9a) shows decreasing Ba contents with increasing $^{87}Sr/^{86}Sr$. On the other hand, no correlations are observed for the Sr vs $^{87}Sr/^{86}Sr$ plot (Fig. 9b) This suggests that the Hemasil syenite parental magma was contaminated by another source that was less Ba-rich but had a similar Sr content. Thus the strong

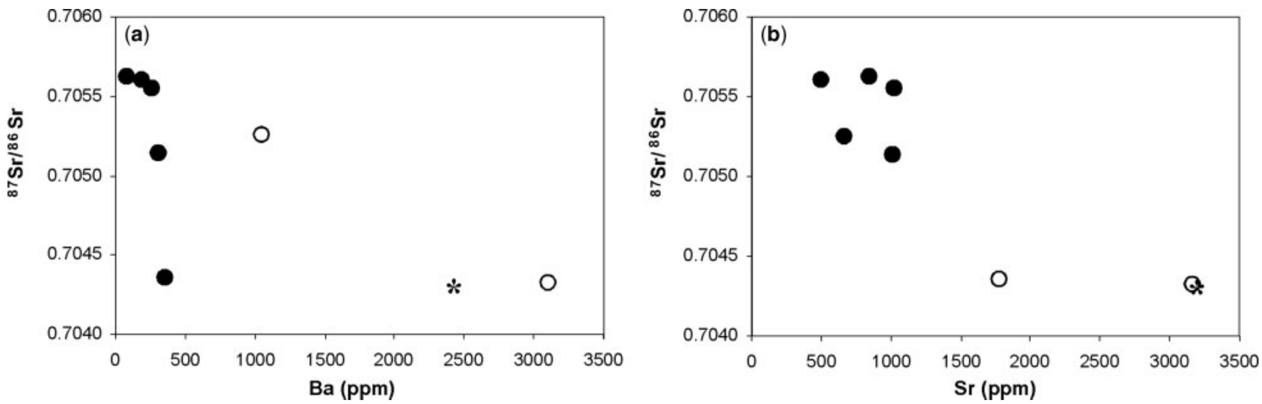

Fig. 9. Relationships between (a) Ba and (b) Sr concentrations and $^{87}Sr/^{86}Sr$ for the Hemasil syenite and the associated lamprophyre. The samples showing evidence of fluid remobilization in Fig. 8 are indicated by open symbols. Same symbols as in Fig. 4.

LILE enrichment of the Hemasil syenite is an original, magmatic feature. This interpretation is also supported by the similarity between the mantle-normalized multi-element diagrams of the syenite and those of the Paleogene Teru volcanics (Fig. 3c). The Teru volcanics were emplaced during the Paleogene in the northern part of the Kohistan arc, ~200 km west of Hemasil, and have the same isotopic composition as the Hemasil syenite ($^{87}Sr/^{86}Sr_{(i)} = 0{\cdot}7050–0{\cdot}7040$ and $\varepsilon_{Nd(i)} = +3{\cdot}3$ to $+5{\cdot}2$; Khan *et al.*, 2004). They are interpreted to have been extracted from a previously metasomatized mantle source (Khan *et al.*, 2004).

The Hemasil syenite and its associated lamprophyre are characterized by unusually radiogenic Hf relative to their Nd isotopic compositions (Fig. 5). This feature, coupled with high Ce/Pb (1·2–8·7), is inferred to reflect possible contamination of the Hemasil mantle source by partial melts derived from oceanic sediments, presumably during subduction of the Neo-Tethys. Contamination of the mantle source by a component of sedimentary origin has also been invoked for the Teru volcanics on the basis of Pb isotope data (Khan *et al.*, 2004).

It is difficult to infer the mineralogical composition of the mantle source of the Hemasil syenite because the rocks are not primitive. As the associated lamprophyre shares the same Sr, Nd, and Hf isotopic compositions, it is considered to have been extracted from a similar source. However, with an Mg-number of 0·42, the lamprophyre composition may itself have been modified by crustal assimilation or fractional crystallization. The Hemasil lamprophyre has a moderate La/Yb ratio (16·8) together with high Y and Yb contents (32·9 ppm and 2·04 ppm, respectively), ruling out the presence of residual garnet. The intermediate La/Yb ratio and the lack of a Eu anomaly further suggest that there was no residual plagioclase in the source, and are consistent with partial melting having occurred in the spinel lherzolite stability field.

To summarize, it is proposed that the source of the Hemasil syenite was a spinel-peridotite strongly depleted, on a time-integrated basis, in Rb, Nd and Hf relative to, respectively, Sr, Sm and Lu, that was enriched at the time of, or shortly prior to, magma generation, thereby preserving the depleted isotopic signature. By comparison with nearby magmatic rocks, such as the Teru volcanics (Khan *et al.*, 2004), the Hemasil syenite and associated lamprophyre are interpreted to result from melting of relic supra-subduction lithospheric or asthenospheric mantle at relatively shallow depth. The difference between the isotopic composition of the Hemasil syenite and the south Karakorum lamprophyres implies that the mantle segment that acted as a source for the syenite did not experience the metasomatic event associated with the generation of the lamprophyres and the southern Tibetan ultrapotassic and potassic magmatic rocks.

GEODYNAMIC MODELS FOR THE SOUTH KARAKORUM AND SOUTHERN TIBET MAGMATISM

Origin of the ultrapotassic and potassic magmatism

As pointed out in the previous section, the contemporaneous south Karakorum lamprophyres and southern Tibetan ultrapotassic and potassic rocks share many geochemical and isotopic characteristics (see Figs 2–4) and define a nearly continuous belt south of the Indus–Tsangpo Suture Zone (Fig. 1). This in turn suggests that they might be related through a common geodynamic event. Moreover, the main geodynamic processes that have been proposed to explain the late orogenic potassic and ultrapotassic magmatism (i.e. convective thinning, continental subduction and slab break-off) all operate at the scale of the orogen. Consequently, in the following discussion the contemporaneous south Karakorum lamprophyres and southern Tibetan potassic and ultrapotassic rocks will be treated as belonging to the same magmatic event.

The presence of lamprophyres and ultrapotassic and potassic rocks in south Karakorum and southern Tibet, respectively, suggests derivation from an enriched reservoir in the shallow Asian, most probably lithospheric, mantle. The most primitive mantle-derived melts (excluding the adakitic melts), emplaced along the south Asian active margin from south Karakorum to southern Tibet between ~120 and ~35 Ma, have similar isotopic compositions with ε_{Nd} varying from about +3 to +6 and $^{87}Sr/^{86}Sr$ at about 0·705 (Allègre *et al.*, 1980; Harris *et al.*, 1988; Petterson *et al.*, 1993; Khan *et al.*, 1997, 2004; Miller *et al.*, 2000; Rolland *et al.*, 2000, 2002*b*), indicative of derivation from time-integrated depleted mantle reservoirs. A significant change happened at around ~25 Ma, the age of the oldest ultrapotassic magmatic rocks from southern Tibet (Miller *et al.*, 1999). Indeed, the Neogene magmatic rocks are clearly distinct from their Cretaceous counterparts, probably as a result of changes in the India–Asia convergent zone geodynamics, and/or in the supra-subduction Asian lithospheric and/or asthenospheric mantle composition.

The origin of the Neogene ultrapotassic and potassic magmatic rocks in southern Tibet and south Karakorum may be related to several geodynamic events: convective thinning of the lithospheric root, continental subduction, or break-off of the subducted Indian continental margin or Indian oceanic lithosphere initially attached to the continental margin. Based on our new data, we will assess each of these models.

(1) Thinning of the lithospheric mantle may occur as a consequence of gravitational instability produced in response to lithospheric thickening (Houseman *et al.*, 1981; Houseman & Molnar, 1997; Conrad & Molnar, 1999). The detachment of the unstable layer can take place either at the Moho (mantle lithosphere delamination) or within the lithospheric mantle itself (convective removal of the basal layer of the lithosphere). Following detachment, the sinking portion of the lithosphere is replaced by hot rising asthenospheric mantle. The juxtaposition of this hot mantle material with either the remaining lithosphere or the lower crust triggers melting in the overlying domains (Turner *et al.*, 1992). Partial melting may also occur in the uprising asthenosphere, as a result of adiabatic decompression at shallow depth (<50 km; Davies & van Blanckenburg, 1995). In the case of south Karakorum and southern Tibet, the presence of thick continental crust and the occurrence of magmas derived from enriched mantle sources do not favour wholesale mantle delamination and therefore convective removal of only a part of the Asian lithospheric mantle has been invoked (Houseman *et al.*, 1981; Turner *et al.*, 1996). An important limitation of the convective thinning model is related to the size and shape of the zone of magmatic activity. This zone stretches along the Indus–Tsangpo Suture Zone (Fig. 1) for more than 2000 km and forms a relatively narrow belt (~150 km across). Based on geophysical data, numerous gravitational instabilities have been recognized worldwide (see Houseman & Molnar, 2001, for a review). For example, in the Transverse Range (California) and in the Southern Alps (New Zealand), the instabilities are relatively small, ~200 km long and 60–80 km wide for the Transverse Range (Kohler, 1999) and ~300 km long and ~80 km wide in New Zealand (Stern *et al.*, 2000). In areas such as the Alboran Sea, the Tien Shan, and northern Tibet, lithospheric thinning associated with removal of part of the mantle lithosphere is strongly suggested by both geophysical and geochemical data (see Houseman & Molnar, 2001, for review). In these regions, the igneous rocks do not have linear trends, but are spread over broad domains, specifically, an ~200 km × 300 km zone in Tien Shan (Sobel & Arnaud, 2000), an ~200 km × 200 km zone in the Alboran Sea (Turner *et al.*, 1999), and an ~400 km × 1000 km zone in northern Tibet (Chung *et al.*, 2005). Houseman & Molnar (2001) further inferred that lithospheric thinning may have occurred beneath the northern part of the Tibetan plateau, where magmatism initiated at ~13 Ma (Turner *et al.*, 1996), rather than under the southern part. However, several workers have suggested that the northern Tibetan magmatism is related to continental subduction (Guo *et al.*, 2006; Ding *et al.*, 2007; Wang *et al.*, 2008). Recent analysis of shear-wave velocity beneath Tibet by McKenzie & Priestley (2008) suggests that the present-day lithosphere is more than 200 km thick beneath the whole of the Tibetan plateau and the Karakorum. Thus, there is no geophysical evidence for lithospheric thinning beneath south Tibet and south Karakorum. Based on this observation, along with the elongated shape of the Neogene igneous belt in south Karakorum and southern Tibet, a model related to lithospheric thinning seems unlikely to be able to account for the Neogene ultrapotassic and potassic magmatic rocks.

(2) Another model proposed to explain the southern Tibet Neogene magmatism is based on continental subduction (Arnaud *et al.*, 1992; Ding *et al.*, 2003). According to this model, fluids released by the subducting Indian continental crust would have caused metasomatic changes in the overriding Asian mantle and triggered partial melting. This model has the advantage of accounting for both the extent of the magmatic rocks along a narrow zone parallel to the ITSZ and the isotopic signature of the southern Tibetan and south Karakorum Neogene magmatic rocks, suggesting mixing between the Cretaceous–Paleogene Asian mantle and fluids from the Indian crust (Fig. 4). However, continental subduction was already active at 55 Ma (de Sigoyer *et al.*, 2000; Guillot *et al.*, 2003) and

metasomatism of the Asian upper mantle wedge by fluids or melts from the Indian crust occurred between 55 and 45 Ma (Guillot *et al.*, 2001; Hattori & Guillot, 2007). Thus, if magmatism related to continental subduction took place it is expected to have started earlier than the south Karakorum and south Tibetan Neogene igneous episode.

(3) More recently, break-off of the continental Indian slab has been proposed as an alternative model (Miller *et al.*, 1999; Chemenda *et al.*, 2000; Mahéo *et al.*, 2002; Hou *et al.*, 2004; Williams *et al.*, 2004). In this model, part of the subducting Indian lithosphere becomes detached, thereby creating a gap into which the asthenospheric mantle can rise, until it reaches the overlying lithospheric or asthenospheric mantle of the Asian plate and triggers partial melting. This model accounts readily for the location of the magmatic activity along a narrow zone parallel to the ITSZ. Tomographic studies clearly show that the already subducted Indian continental margin and the Neo-Tethyan oceanic slab form two separate geophysical anomalies in the upper mantle (Van der Voo *et al.*, 1999; Negredo *et al.*, 2007), thereby providing evidence that a slab break-off event has occurred. Moreover, detailed analysis of these data by Negredo *et al.* (2007) suggested that such detachment occurred at about 45 Ma, as previously proposed by Chemenda *et al.* (2000) and Kohn & Parkinson (2002). This could explain the occurrence of Eocene magmatic rocks with the same isotopic and chemical signatures as the magmatic rocks emplaced during the Cretaceous subduction of the Neo-Tethys Ocean.

The inferred slab break-off episode would have induced partial melting of the Asian mantle by heat advection coming from asthenospheric mantle upwelling (Fig. 10b). This event could also account for the dramatic decrease in the India–Asia convergence rate (from ~100 to ~60 mm/year) that took place at ~45 Ma. The occurrence of slab break-off ~10 Myr after the initiation of Indian continental subduction is also in good agreement with numerical modelling of break-off timescales (Van de Zedde & Wortel, 2001; Brouwer *et al.*, 2004). However, an ~45 Ma break-off event cannot easily account for the Neogene magmatism, and a model based on a single break-off event as proposed by Mahéo *et al.* (2002) is not realistic. For this reason a second slab break-off within the Indian continental margin lithosphere might be postulated. The occurrence of multiple breaks-off within subducting oceanic lithosphere has been proposed by Gerya *et al.* (2004), based on numerical modelling. Moreover, analogue modelling by Chemenda *et al.* (2000) of Indian continental subduction following oceanic subduction produced two successive break-off events, the second one occurring within the subducting continental lithosphere. Tomographic data suggest that several remnants of detached slabs are present beneath the India–Asia convergence zone (Van der Voo *et al.*, 1999). DeCelles *et al.* (2002) have suggested that the two shallower anomalies correspond to the detached Neo-Tethyan subducted slab and to a portion of the subducted Indian continental margin, respectively; Replumaz *et al.* (in preparation) have inferred that the shallowest anomaly detached at 25 ± 5 Ma. This second break-off of the subducting Indian continental lithosphere could have induced partial melting of the Asian mantle wedge previously metasomatized by melts or fluids derived from subducted Indian crustal components, and could account for the Neogene south Karakorum and south Tibetan magmatism (Fig. 10d). A progressive increase in the age of initiation and termination of this magmatic episode from south Karakorum and east of Lhasa toward south–central Tibet (Chung *et al.*, 2005) suggests that this break-off could have started in Karakorum and east of Lhasa and propagated eastward and westward, respectively. Such an evolutionary history would also be compatible with the study of Mugnier & Huyghe (2006), who proposed that the isostatic rebound of the central Himalayas at ~15 Ma on the one hand, and the Ganges basin geometry on the other hand, are controlled by the break-off of the Indian continental lithosphere. Moreover, following slab break-off, the highly buoyant remnants of the undetached continental lower plate could have progressively risen and underplated the base of the crust of the Asian plate (Fig. 10e; Chemenda *et al.*, 2000; Zhou & Murphy, 2005) such as observed in south Tibet today.

Relationship between the lamprophyres and the Baltoro granitoids

The similar emplacement ages of the granitoids and lamprophyres suggest a possible genetic relationship between them, although the Baltoro batholith could be the result of thermal re-equilibration by radioactive heating of the previously thickened crust. As discussed above, the generation of this batholith is interpreted in terms of partial melting of south Karakorum Cretaceous calc-alkaline basaltic or dioritic rocks. Based on pressure estimates in the contact aureole of the batholith, Searle *et al.* (1992) proposed that the minimum depth of melting of the Baltoro granitoids source was at about 30 km. At such depths and down to 60 km, melting of basaltic or dioritic rocks can occurs at 650–700°C (H_2O-saturated solidus) producing a garnet + amphibole residue (Rapp & Watson, 1995). In a scenario of crustal thickening by a factor of two, temperatures of 650°C would be reached at ~30 km depth after ~60 Myr of thermal re-equilibration and at ~60 km depth after 30 Myr (Thompson & Connolly, 1995). Consequently, thermal re-equilibration of the thickened Karakorum crust alone cannot explain the formation of the Baltoro batholith. Additional heat could be provided by shear heating along major strike-slip faults (Leloup *et al.*, 1999), such as the nearby Karakorum Fault (Fig. 1).

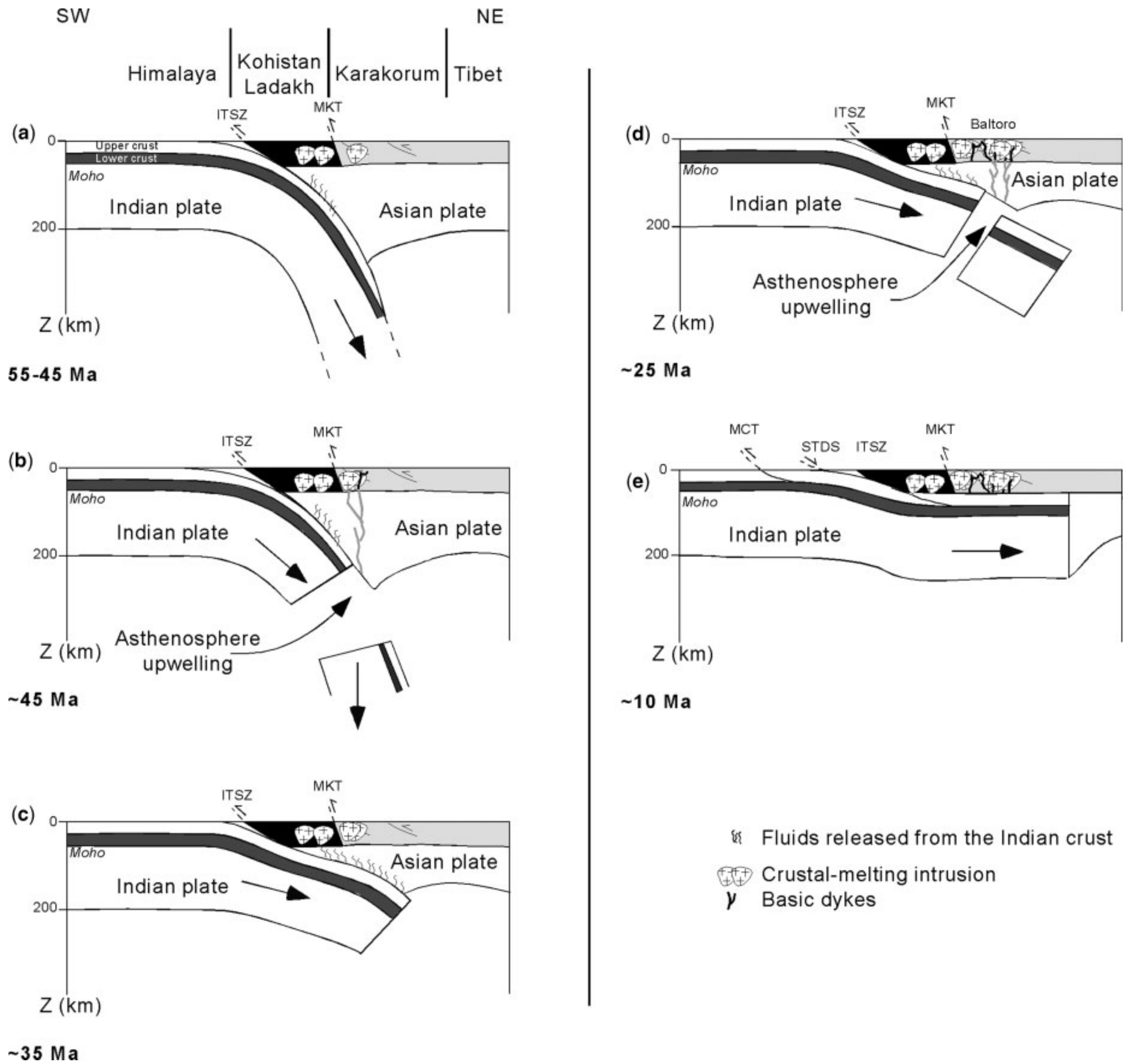

Fig. 10. Proposed evolutionary scheme for the India–Asia convergence zone in the Karakorum region during Tertiary times. (a) Early Eocene northward subduction of the Indian continental lithosphere. Subduction-related magmatism is still active. (b) Eocene break-off of the Indian lithosphere and associated Asian lithospheric mantle melting. (c) Eocene–Early Oligocene low-angle continental subduction. (d) Early Oligocene second break-off event, occurring within the Indian continental lithosphere and triggering the generation of Neogene potassic–ultrapotassic magmatism and crustal melting. (e) Miocene underthrusting of the Indian lithosphere beneath the Asian lithosphere. ITSZ, Indus–Tsangpo Suture Zone; MCT, Main Central Thrust; MKT, Main Karakorum Thrust; STDS, South Tibetan Detachment System.

However, although part of the Baltoro batholith is located on this fault, its western extension crops out more than 100 km away from it. The fault is inferred to be a lithosphere-scale structure that might have guided magma ascent (a 'leaky' transcurrent fault) and facilitated heat transfer by advection of mantle-derived, lamprophyric magmas (Fig. 10d). The actual volume of lamprophyric melts intruded into the south Karakorum crust or underplated beneath it cannot readily be resolved. However, in the context of warm lower and middle crust as a result of thermal re-equilibration, large volumes of mafic melts are not required. Moreover, during a slab break-off event, asthenospheric rise into the resulting gap could also increase the temperature of the crust above the subducting slab (Van de Zedde & Wortel, 2001), especially if break-off occurred at shallow depths and if the overriding crust is thick, both of which seem to be the case in southern Karakorum.

Origin of the Hemasil magmatism

Based on the previous data, the Hemasil syenite and associated lamprophyre are interpreted to reflect partial melting of a relic of the shallow (in the spinel-peridotite stability field), metasomatized mantle of the Asian plate. The Hemasil syenite is located along the Shigar Fault, a currently inactive, crustal-scale dextral strike-slip fault (Mahéo *et al.*, 2004). There are numerous examples of spatial associations between alkaline rocks and major strike-slip faults, such as the Gar syenite along the Karakorum Fault (Miller *et al.*, 2000), the Red River Fault Zone (Zhang & Schärer, 1999), the Central Anatolian Fault Zone (Parlak *et al.*, 2001), the North Anatolian Fault (Adiyaman *et al.*, 2001), the Alpine Fault in New Zealand (Adams & Cooper, 1996), and also in several orogens such as the Rif and the Atlas (Beraaouz & Bonin, 1993) and the Carpathian area (Seghedi *et al.*, 1998). In these regions, part if not all of the magma genesis is associated with mantle decompression along the fault plane during transtensional events and subsequent adiabatic partial melting (Seghedi *et al.*, 1998; Miller *et al.*, 2000; Adiyaman *et al.*, 2001; Parlak *et al.*, 2001; Guo *et al.*, 2005). The magmatic fabric and ductile deformation of the Hemasil syenite are indicative of emplacement during strike-slip faulting along the Shigar Fault (Lemennicier *et al.*, 1996; Mahéo *et al.*, 2004). On this basis, we propose that the generation of the Hemasil syenite and associated lamprophyre is also related to mantle upwelling and adiabatic decompression in a transtensive segment of the Shigar Fault. Analyses of available structural data (Le Fort *et al.*, 1995; Lemennicier, 1996; Lemennicier *et al.*, 1996; Rolland *et al.*, 2001; Mahéo *et al.*, 2004; Pêcher *et al.*, 2008) are compatible with the Hemasil syenite being localized in a transtensional pull-apart zone along the dextral strike-slip Shigar Fault. Additional heat may have been provided by the lamprophyric melts as well as by shear heating along the Shigar Fault.

The mantle source of the Hemasil syenite has not been affected by the metasomatic event associated with the generation of the 22–24 Ma lamprophyre and could represent the uppermost part of the Asian mantle wedge or a relic of the mantle section of the Cambro-Ordovician Masherbrum greenstone belt as evidenced by the similarity of their isotopic composition.

CONCLUSIONS

Three major igneous stages can be recognized in south Karakorum and southern Tibet, as follows.

(1) During the first stage, from the Cretaceous to the Paleogene, magmas were produced by partial melting of slightly metasomatized supra-subduction zone lithospheric and asthenospheric Asian mantle. This occurred during a protracted period of oceanic subduction (~120–55 Ma), and then during a shorter continental subduction stage (from 55 to ~45 Ma, Fig. 10a). This was followed by break-off of the Indian lithosphere (~45 Ma, Fig. 10b), which caused further magmatic activity associated with variable degrees of interaction with the Asian crust.

(2) The second stage occurred from 25 to 8 Ma, and was characterized by the emplacement of ultrapotassic and potassic magmas. This igneous phase is interpreted to reflect partial melting of remnants of the Asian lithospheric mantle trapped between the Asian crust and the underthrust Indian continental margin lithosphere after a second slab break-off event (Fig. 10d). The trapped Asian lithospheric mantle had been modified by interaction with fluids released from the subducting Indian continental crust and its cover sediments (Fig. 10c). The intrusion of mantle melts into the previously thickened crust induced partial melting of both the southern Tibetan and the south Karakorum mafic lower crust (Fig. 10d) and generated the high Sr–Ba granitoids of the Baltoro batholith. Following slab break-off, the highly buoyant remnants of the continental lower plate could have progressively risen and underplated the base of the crust of the Asian plate (Fig. 10e).

(3) The last igneous stage (8–9 Ma) is documented in south Karakorum by the synkinematic emplacement of the Hemasil syenite along the Shigar strike-slip fault. This LILE- and LREE-enriched, but isotopically (Sr–Nd–Hf) depleted body is interpreted to have been generated by decompression melting of portions of time-integrated depleted mantle that experienced recent enrichment along a transtensive segment of the fault. In addition to decompression, local high geothermal gradients produced by the intrusion of the lamprophyres as well as shear heating along the Shigar Fault may have contributed to trigger partial melting.

ACKNOWLEDGEMENTS

The authors thank F. Debon for providing the Baltoro samples and some unpublished geochemical data. We also thank C. Douchet, P. Capiez, and P. Telouk for technical assistance. Discussion with Y. Rolland, N. Arnaud, J. P. Avouac, and P. Luffi helped improve the manuscript, which also benefited from reviews by Z. Guo, Y. Niu, U. Schaltegger, H. Williams and M. Wilson. Financial support from the INSU DYETI program is gratefully acknowledged.

REFERENCES

Adams, C. J. & Cooper, A. F. (1996). K–Ar age of a lamprophyre dike swarm near Lake Wanaka, west Otago, South Island, New Zealand. *New Zealand Journal of Geology and Geophysics* **39**, 17–23.

Adiyaman, O., Chorowicz, J., Arnaud, O. N., Gundogdu, M. N. & Gourgaud, A. (2001). Late Cenozoic tectonics and volcanism along the North Anatolian Fault: new structural and geochemical data. *Tectonophysics* **338**, 135–165.

Albarède, F., Simonetti, T., Vervoort, J., Blichert-Toft, J. & Abouchami, W. (1998). A Hf–Nd isotopic correlation in ferromanganese nodules. *Geophysical Research Letters* **25**, 3895–3898.

Aldanmaz, E., Pearce, J. A., Thirlwall, M. F. & Mitchell, J. G. (2000). Petrogenetic evolution of late Cenozoic, post-collision volcanism in western Anatolia, Turkey. *Journal of Volcanology and Geothermal Research* **102**, 67–95.

Allègre, C. J. & Othman, D. B. (1980). Nd–Sr isotopic relationship in granitoid rocks and continental-crust development—a chemical approach to orogenesis. *Nature* **286**, 335–342.

Arnaud, N. O., Vidal, P., Tapponier, P., Matte, P. & Deng, W. M. (1992). The high K_2O volcanism of northwestern Tibet: geochemistry and tectonic implications. *Earth and Planetary Science Letters* **111**, 351–367.

Barry, T. L., Saunders, A. D., Kempton, P. D., Windley, B. F., Pringle, M. S., Dorjnamjaa, D. & Saandar, S. (2003). Petrogenesis of Cenozoic basalts from Mongolia: Evidence for the role of asthenospheric versus metasomatized lithospheric mantle sources. *Journal of Petrology* **44**, 55–91.

Beard, B. L. & Johnson, C. M. (1993). Hf isotope composition of late Cenozoic basaltic rocks from northwestern Colorado, USA—new constraints on mantle enrichment processes. *Earth and Planetary Science Letters* **119**, 495–509.

Beraaouz, E. & Bonin, B. (1993). Within-continent alkaline magmatism related to strike-slip movements—the Mesozoic plutonic complex of Tirrhist, Haut-Atlas (Morocco). *Comptes Rendus de l'Académie des Sciences* **317**, 647–653.

Bertrand, J. M., Kienast, J. R. & Pinardon, J. L. (1988). Structure and metamorphism of the Karakorum gneisses in the Braldu–Baltoro valley (north Pakistan). *Geodinamica Acta* **2**, 135–50.

Blichert-Toft, J. (2001). On the Lu–Hf isotope geochemistry of silicate rocks. *Geostandards Newsletter* **25**, 41–46.

Blichert-Toft, J. & Albarède, F. (1997). The Lu–Hf geochemistry of chondrites and the evolution of the mantle–crust system. *Earth and Planetary Science Letters* **148**, 243–258.

Blichert-Toft, J., Chauvel, C. & Albarède, F. (1997). Separation of Hf and Lu for high precision isotope analysis of rocks samples by magnetic sector-multiple collector ICP-MS. *Contributiosn to Mineralogy and Petrology* **127**, 248–260.

Blichert-Toft, J., Frey, F. A. & Albarede, F. (1999). Hf isotope evidence for pelagic sediments in the source of Hawaiian basalts. *Science* **285**, 879–882.

Bonin, B. (1988). From orogenic to anorogenic environments: evidence from associated magmatic episodes. *Schweizerische Mineralogische und Petrographische Mitteilungen* **68**, 301–311.

Brouwer, F. M., Van de Zedde, D. M. A., Wortel, M. J. R. & Vissers, R. L. M. (2004). Late-orogenic heating during exhumation: Alpine P–T–t trajectories and thermomechanical models. *Earth and Planetary Science Letters* **220**, 185–199.

Castillo, P. R., Janney, P. E. & Solidum, R. U. (1999). Petrology and geochemistry of Camiguin Island, southern Philippines: insights to the source of adakites and other lavas in a complex arc setting. *Contributions to Mineralogy and Petrology* **134**, 33–51.

Chemenda, A. I., Burg, J. P. & Mattauer, M. (2000). Evolutionary model of the Himalaya–Tibet system: geopoem based on new modelling, geological and geophysical data. *Earth and Planetary Science Letters* **174**, 397–409.

Chung, S. L., Lo, C. H., Lee, T. Y., Zhang, Y. Q., Xie, Y. W., Li, X. H., Wang, K. L. & Wang, P. L. (1998). Diachronous uplift of the Tibetan plateau starting 40 Myr ago. *Nature* **394**, 769–773.

Chung, S. L., Liu, D. Y., Ji, J. Q., *et al*. (2003). Adakites from continental collision zones: Melting of thickened lower crust beneath southern Tibet. *Geology* **31**, 1021–1024.

Chung, S. L., Chu, M. F., Zhang, Y. Q., *et al*. (2005). Tibetan tectonic evolution inferred from spatial and temporal variations in post-collisional magmatism. *Earth-Science Reviews* **68**, 173–196.

Conrad, C. P. & Molnar, P. (1999). Convective instability of a boundary layer with temperature- and strain-rate-dependent viscosity in terms of 'available buoyancy'. *Geophysical Journal International* **139**, 51–68.

Coulon, C., Maluski, H., Bollinger, C. & Wang, S. (1986). Mesozoic and Cenozoic volcanic rocks from central and southern Tibet: ^{39}Ar–^{40}Ar dating, petrological characteristics and geodynamical signifiance. *Earth and Planetary Science Letters* **79**, 281–302.

Coulon, C., Megartsi, Mh, Fourcade, S., Maury, R. C., Bellon, H., Louni-Hacini, A., Cotten, J., Coutelle, A. & Hermitte, D. (2002). Post-collisional transition from calc-alkaline to alkaline volcanism during the Neogene in Oranie (Algeria): magmatic expression of a slab breakoff. *Lithos* **62**, 87–110.

Crawford, M. B. & Searle, M. P. (1992). Field relationships and geochemistry of pre-collisional (India–Asia) granitoid magmatism in the central Karakoram, northern Pakistan. *Tectonophysics* **206**, 171–192.

Crawford, M. B. & Searle, M. P. (1993). Collision-related granitoid magmatism and crustal structure of the Hunza Karakoram, north Pakistan. In: Treloar, P. J. & Searle, M. P. (eds) *Himalayan Tectonics. Geological Society, London, Special Publications* **74**, 53–68.

Davies, J. H. & van Blanckenburg, F. (1995). Slab breakoff: a model of lithosphere detachment and its test in the magmatism and deformation of collisional orogens. *Earth and Planetary Science Letters* **129**, 85–102.

Debon, F. (1995). Incipient India–Eurasia collision and plutonism: The Lower Cenozoic Batura granites (Hunza Karakorum, North Pakistan). *Journal of the Geological Society, London* **152**, 785–795.

Debon, F. & Khan, A. (1996). Alkaline orogenic plutonism in the Upper Cretaceous Koz Sar complex (Karambar valley, N. Pakistan). *Geodinamica Acta* **9**, 145–160.

Debon, F., Zimmermann, J. L. & Bertrand, J. M. (1986). The Baltoro Granite (Karakoram axial batholith, northern Pakistan)—an Upper Miocene subalkaline intrusion. *Comptes Rendus de l'Académie des Sciences* **303**, 463–466.

Debon, F., LeFort, P., Dautel, D., Sonet, J. & Zimmermann, J. L. (1987). Granites of western Karakorum and northern Kohistan (Pakistan): a composite Mid-Cretaceous to upper Cenozoic magmatism. *Lithos* **20**, 19–40.

DeCelles, P. G., Robinson, D. M. & Zandt, G. (2002). Implications of shortening in the Himalayan fold–thrust belt for uplift of the Tibetan Plateau. *Tectonics* **21**, doi:10.1029/2001TC001322.

Deniel, C., Vidal, P., Fernandez, A., Lefort, P. & Peucat, J. J. (1987). Isotopic study of the Manaslu Granite (Himalaya, Nepal)—inferences on the age and source of Himalayan leucogranites. *Contributions to Mineralogy and Petrology* **96**, 78–92.

de Sigoyer, J., Chavagnac, V., Blichert-Toft, J., Villa, I. M., Luais, B., Guillot, S., Cosca, M. & Masclem, G. (2000). Dating the Indian continental subduction and collisional thickening in the Northwest Himalaya; multichronology of the Tso Morari eclogites. *Geology* **28**, 487–490.

Ding, L., Kapp, P., Zhong, D. L. & Deng, W. M. (2003). Cenozoic volcanism in Tibet: Evidence for a transition from oceanic to continental subduction. *Journal of Petrology* **44**, 1833–1865.

Ding, L., Kapp, P., Yue, Y. H. & Lai, Q. Z. (2007). Postcollisional calc-alkaline lavas and xenoliths from the southern Qiangtang terrane, central Tibet. *Earth and Planetary Science Letters* **254**, 28–38.

Fraser, J. E., Searle, M. P., Parrish, R. R. & Noble, S. R. (2001). Chronology of deformation, metamorphism, and magmatism in the southern Karakoram Mountains. *Geological Society of America Bulletin* **113**, 1443–1455.

Frost, B. R., Barnes, C. G., Collins, W. J., Arculus, R. J., Ellis, D. J. & Frost, C. D. (2001). A geochemical classification for granitic rocks. *Journal of Petrology* **42**, 2033–2048.

Gaetani, M., LeFort, P., Tanoli, S., Angiolini, L., Nicora, A., Sciunnach, D. & Khan, A. (1996). Reconnaissance geology in upper Chitral, Baroghil and Karambar districts (northern Karakorum, Pakistan). *Geologische Rundschau* **85**, 683–704.

Gao, Y. F., Hou, Z. Q., Kamber, B. S., Wei, R. H., Meng, X. J. & Zhao, R. S. (2007). Lamproitic rocks from a continental collision zone: Evidence for recycling of subducted Tethyan oceanic sediments in the mantle beneath southern Tibet. *Journal of Petrology* **48**, 729–752.

Gerya, T. V., Yuen, D. A. & Maresch, W. V. (2004). Thermomechanical modelling of slab detachment. *Earth and Planetary Science Letters* **226**, 101–116.

Godfrey, L. V., Lee, D. C., Sangrey, W. F., Halliday, A. N., Salters, V. J. M., Hein, J. R & White, W. M. (1997). The Hf isotopic composition of ferromanganese nodules and crusts and hydrothermal manganese deposits: Implications for seawater Hf. *Earth and Planetary Science Letters* **151**, 91–105.

Guillot, S. (1993). Le granite du Manaslu (Népal Central), marqueur de la subduction et de l'extension intracontinentales himalayennes. PhD thesis, Université Joseph Fourier, Grenoble, 97 pp.

Guillot, S. & Le Fort, P. (1995). Geochemical constraints on the bimodal origin of High Himalayan leucogranites. *Lithos* **35**, 221–234.

Guillot, S., Hattori, K. H., de Sigoyer, J., Nagler, T. & Auzende, A. L. (2001). Evidence of hydration of the mantle wedge and its role in the exhumation of eclogites. *Earth and Planetary Science Letters* **193**, 115–127.

Guillot, S., Garzanti, E., Baratoux, D., Marquer, D., Maheo, G. & de Sigoyer, J. (2003). Reconstructing the total shortening history of the NW Himalaya. *Geochemistry, Geophysics, Geosystems* **4**, doi:10.1029/2002GC000484.

Guo, Z. F., Hertogen, J., Liu, J. Q., Pasteels, P., Boven, A., Punzalan, L., He, H. Y., Luo, X. J. & Zhang, W. H. (2005). Potassic magmatism in western Sichuan and Yunnan Provinces, SE Tibet, China: Petrological and geochemical constraints on petrogenesis. *Journal of Petrology* **46**, 33–78.

Guo, Z. F., Wilson, M., Liu, J. Q. & Mao, Q. (2006). Post-collisional, potassic and ultrapotassic magmatism of the northern Tibetan Plateau: Constraints on characteristics of the mantle source, geodynamic setting and uplift mechanisms. *Journal of Petrology* **47**, 1177–1220.

Guo, Z. F., Wilson, M. & Liu, J. Q. (2007). Post-collisional adakites in south Tibet: Products of partial melting of subduction-modified lower crust. *Lithos* **96**, 205–224.

Harris, N. B., Xu, R., Lewis, C. L., Hawkesworth, C. J. & Zhang, Y. (1988). Isotope geochemistry of the 1985 Tibet Geotraverse, Lhasa to Golmud. *Philosophical Transactions of the Royal Society of London* **327**, 263–285.

Harris, N. B. W., Kelley, S. & Okay, A. I. (1994). Postcollision Magmatism and Tectonics in Northwest Anatolia. *Contributions to Mineralogy and Petrology* **117**, 241–252.

Hattori, K. H. & Guillot, S. (2007). Geochemical character of serpentinites associated with high- to ultrahigh-pressure metamorphic rocks in the Alps, Cuba, and the Himalayas: Recycling of elements in subduction zones. *Geochemistry, Geophysics, Geosystems* **8**, doi:10.1029/2007GC001594.

Hernandez, J., Larouziere, F. D., Bolze, J. & Bordet, P. (1987). Le magmatisme néogène bético-rifain et le couloir de décrochement trans-Alboran. *Bulletin de la Société Géologique de France* **8**, 257–267.

Heuberger, S., Schaltegger, U., Burg, J.-P., Villa, I. M., Frank, M., Dawood, H., Hussain, S. & Zanchi, A. (2007). Age and isotopic constraints on magmatism along the Karakoram–Kohistan Suture Zone, NW Pakistan: evidence for subduction and continued convergence after India–Asia collision. *Swiss Journal of Geosciences* **100**, 85–107.

Hildebrand, P. R., Noble, S. R., Searle, M. P. & Parrish, R. R. (1998). Tectonic significance of 24 Ma crustal melting in the eastern Hindu Kush, Pakistan. *Geology* **26**, 871–874.

Hou, Z. Q., Gao, Y. F., Qu, X. M., Rui, Z. Y. & Mo, X. X. (2004). Origin of adakitic intrusives generated during mid-Miocene east–west extension in southern Tibet. *Earth and Planetary Science Letters* **220**, 139–155.

Houseman, G. A. & Molnar, P. (1997). Gravitational (Rayleigh–Taylor) instability of a layer with non-linear viscosity and convective thinning of continental lithosphere. *Geophysical Journal International* **128**, 125–150.

Houseman, G. & Molnar, P. (2001). Mechanisms of lithospheric rejuvenation associated with continental orogeny. In: Miller, J. A., Holdsworth, R. E., Buick, I. S. & Hand, M. (eds) *Continental Reactivation and Reworking. Geological Society, London, Special Publications* **184**, 13–38.

Houseman, G. A., McKenzie, D. P. & Molnar, P. (1981). Convective instability of a thickened boundary layer and its relevance for the thermal evolution of continental convergent belts. *Journal of Geophysical Research* **86**, 6115–6132.

Inger, S. & Harris, N. (1993). Geochemical constraints on leucogranite magmatism in the Langtang valley, Nepal Himalaya. *Journal of Petrology* **34**, 345–368.

Jacobsen, S. B. & Wasserburg, G. J. (1980). Sm–Nd isotopic evolution of chondrites. *Earth and Planetary Science Letters* **50**, 139–155.

Jagoutz, O., Muntener, O., Burg, J. P., Ulmer, P. & Jagoutz, E. (2006). Lower continental crust formation through focused flow in km-scale melt conduits: The zoned ultramafic bodies of the Chilas complex in the Kohistan island arc (NW Pakistan). *Earth and Planetary Science Letters* **242**, 320–342.

Johnson, C. M. & Beard, B. L. (1993). Evidence from hafnium isotopes for ancient sub-oceanic mantle beneath the Rio Grande Rift. *Nature* **362**, 441–444.

Kagami, H., Ulmer, P., Hansmann, W., Dietrich, V. & Steiger, R. H. (1991). Nd–Sr isotopic and geochemical characteristics of the southern Adamello (northern Italie) intrusive: implication for crustal versus mantle origin. *Journal of Geophysical Research* **96**, 14331–14346.

Khan, M. A., Stern, R. J., Gribble, R. F. & Windley, B. F. (1997). Geochemical and isotopic constraints on subduction polarity, magma sources, and palaeogeography of the Kohistan intra-oceanic arc, northern Pakistan Himalaya. *Journal of the Geological Society, London* **154**, 935–946.

Khan, S. D., Stern, R. J., Manton, M. I., Copeland, P., Kimura, J. I. & Khan, M. A. (2004). Age, geochemical and Sr–Nd–Pb isotopic constraints for mantle source characteristics and petrogenesis of Teru volcanics, Northern Kohistan Terrane, Pakistan. *Tectonophysics* **393**, 263–280.

Kohler, M. D. (1999). Lithospheric deformation beneath the San Gabriel Mountains in the southern California Transverse Ranges. *Journal of Geophysical Research* **104**, 15025–15041.

Kohn, M. J. & Parkinson, C. D. (2002). Petrologic case for Eocene slab breakoff during the Indo-Asian collision. *Geology* **30**, 591–594.

Le Fort, P., Michard, A., Sonet, J. & Zimmermann, J. L. (1983). Petrography, geochemistry and geochronology of some samples from the Karakorum Axial Batholith (northern Pakistan). In: Shams, F. A. (ed.) *Granites of Himalayas, Karakoram and Hindu Kush*. Lahore: Institute of Geology, Punjab University, pp. 377–387.

Le Fort, P., Tongiorgi, M. & Gaetani, M. (1994). Discovery of a crystalline basement and Early Ordovician marine transgression in the Karakoram Mountain Range, Pakistan. *Geology* **22**, 941–944.

Le Fort, P., Lemennicier, Y., Lombardo, B., Pêcher, A., Pertusati, P., Pognante, U. & Rolfo, F. (1995). Preliminary geological map and description of the Himalaya–Karakorum junction in Chogo Lungma to Turmik area (Baltistan, Northern Pakistan). *Journal of Nepal Geological Society* **11**, 17–38.

Leloup, P. H., Battaglia, J., Ricard, Y. & Lacassin, R. (1999). Shear heating in continental strike-slip shear zones: numerical modelling and case studies. *Geophysical Journal International* **136**, 19–40.

Le Maitre, R. W., Bateman, E., Dudek, P., Keller, A., Lameyre, J., Le Bas, J., Sabine, M. J., Schmid, P. A., Sorensen, R., Streckeisen, H., Woolley, A. R., Zanettin, B. (1989) *A classification of igneous rocks and glossary of terms, recommendations of the International Union of Geological Sciences, Subcommission on the Systematics of Igneous Rocks*. Blackwell Scientific: Oxford.

Lemennicier, Y. (1996). Le complexe métamorphique du Sud Karakorum dans le secteur du Chogo Lungma (Baltistan—Nord Pakistan)—Etude structurale, métamorphique, géochimique et radiochronologique. PhD thesis, Université J. Fourier, Grenoble, 171 pp.

Lemennicier, Y., LeFort, P., Lombardo, B., Pêcher, A. & Rolfo, F. (1996). Tectonometamorphic evolution of the central Karakorum (Baltistan—northern Pakistan). *Tectonophysics* **260**, 119–143.

Mahéo, G., Guillot, S., Blichert-Toft, J., Rolland, Y. & Pêcher, A. (2002). A slab breakoff model for the Neogene thermal evolution of South Karakorum and South Tibet. *Earth and Planetary Science Letters* **195**, 45–58.

Mahéo, G., Pêcher, A., Guillot, S., Rolland, Y. & Delacourt, C. (2004). Exhumation of Neogene gneiss domes between oblique crustal boundary in South Karakorum (NW Himalaya, Pakistan). In: Whitney, D. L., Teyssier, V. & Siddoway, C. S. (eds) *Gneiss Domes in Orogeny. Geological Society of America, Special Papers* **380**, 141–154.

Mahoney, J. J., Frei, R., Tejada, M. L. G., Mo, X. X., Leat, P. T. & Nagler, T. F. (1998). Tracing the Indian Ocean mantle domain through time: Isotopic results from Old West Indian, East Tethyan, and South Pacific seafloor. *Journal of Petrology* **39**, 1285–1306.

McDonough, W. & Sun, S. S. (1995). The composition of the Earth. *Chemical Geology* **120**, 223–253.

McKenzie, D. & Priestley, K. (2008). The influence of lithospheric thickness variations on continental evolution. *Lithos* **102**, 1–11.

Miller, C., Schuster, R., Klötzli, U., Frank, W. & Purtscheller, F. (1999). Post-collisional potassic and ultrapotassic magmatism in SW Tibet: geochemical and Sr–Nd–Pb–O isotopic constraints for mantle source characteristics and petrogenesis. *Journal of Petrology* **40**, 1399–1424.

Miller, C., Schuster, R., Klotzli, U., Frank, W. & Grasemann, B. (2000). Late Cretaceous-Tertiary magmatic and tectonic events in the Transhimalaya batholith (Kailas area, SW Tibet). *Schweizerische Mineralogische Und Petrographische Mitteilungen* **80**, 1–20.

Mo, X. X., Hou, Z. Q., Niu, Y. L., Dong, G. C., Qu, X. M., Zhao, Z. D. & Yang, Z. M. (2007). Mantle contributions to crustal thickening during continental collision: Evidence from Cenozoic igneous rocks in southern Tibet. *Lithos* **96**, 225–242.

Mo, X. X., Niu, Y. L., Dong, G. C., Zhao, Z. D., Hou, Z. Q., Su, Z. & Ke, S. (2008). Contribution of syncollisional felsic magmatism to continental crust growth: A case study of the Paleogene Linzizong volcanic succession in southern Tibet. *Chemical Geology* **250**, 49–67.

Mugnier, J. L. & Huyghe, P. (2006). Ganges basin geometry records a pre-15 Ma isostatic rebound of Himalaya. *Geology* **34**, 445–448.

Negredo, A. M., Replumaz, A., Villasenor, A. & Guillot, S. (2007). Modeling the evolution of continental subduction processes in the Pamir–Hindu Kush region. *Earth and Planetary Science Letters* **259**, 212–225.

Nomade, S., Renne, P. R., Mo, X. X., Zhao, Z. D. & Zhou, S. (2004). Miocene volcanism in the Lhasa block, Tibet: spatial trends and geodynamic implications. *Earth and Planetary Science Letters* **221**, 227–243.

Nowell, G. M., Kempton, P. D., Noble, S. R., Fitton, J. G., Saunders, A. D., Mahoney, J. J. & Taylor, R. N. (1998). High precision Hf isotope measurements of MORB and OIB by thermal ionisation mass spectrometry: insights into the depleted mantle. *Chemical Geology* **149**, 211–233.

Parlak, O., Delaloye, M., Demirkol, C. & Unlugenc, U. C. (2001). Geochemistry of Pliocene/Pleistocene basalts along the Central Anatolian Fault Zone (CAFZ), Turkey. *Geodinamica Acta* **14**, 159–167.

Parrish, R. P. & Tirrul, R. (1989). U–Pb ages of the Baltoro granite, northwest Himalaya, and implications for monazite U–Pb systematics. *Geology* **17**, 1076–1079.

Pêcher, A. & Le Fort, P. (1999). Late Miocene evolution of the Karakorum–Nanga Parbat contact zone (northern Pakistan). In: Macfarlane, A., Sorkhabi, R. B. & Quade, J. (eds) *Himalaya and Tibet; Mountain Roots to Mountain Tops. Geological Society of America, Special Papers* **328**, 145–158.

Pêcher, A., Seeber, L., Guillot, S., *et al*. (2008). Stress field evolution in the northwest Himalayan syntaxis, northern Pakistan. *Tectonics* **27**, TC6005, doi:10.1029/2007TC002252.

Petford, N. & Atherton, M. (1996). Na-rich partial melts from newly underplated basaltic crust: The Cordillera Blanca Batholith, Peru. *Journal of Petrology* **37**, 1491–1521.

Petterson, M. G. & Windley, B. F. (1992). Field relations, geochemistry and petrogenesis of the Cretaceous basaltic Jutal Dykes, Kohistan, northern Pakistan. *Journal of the Geological Society, London* **149**, 107–114.

Petterson, M. G., Crawford, M. B. & Windley, B. F. (1993). Petrogenetic implications of neodymium isotope data from the Kohistan Batholith, north Pakistan. *Journal of the Geological Society, London* **150**, 125–129.

Pin, C. & Santos Zalduegui, J. F. (1997). Sequential separation of light rare-earth elements, thorium and uranium by miniaturized extraction chromatography: Application to isotopic analyses of silicate rocks. *Analytica Chimica Acta* **339**, 79–89.

Pin, C., Telouk, P. & Imbert, J. L. (1995). Direct determination of the samarium–neodymium ratio in geological materials by inductively-coupled plasma quadrupole mass-spectrometry with cryogenic desolvation—comparison with isotope-dilution thermal ionization mass-spectrometry. *Journal of Analytical Atomic Spectrometry* **10**, 93–98.

Pognante, U. (1991). Shoshonitic and ultrapotassic postcollisional dykes from northern Karakoram (Sinkiang, China). *Lithos* **26**, 305–316.

Qu, X. M., Hou, Z. Q. & Li, Y. G. (2004). Melt components derived from a subducted slab in late orogenic ore-bearing porphyries in the Gangdese copper belt, southern Tibetan plateau. *Lithos* **74**, 131–148.

Rapp, R. P. & Watson, E. B. (1995). Dehydration melting of metabasalt at 8–32 kbar—implications for continental growth and crust–mantle recycling. *Journal of Petrology* **36**, 891–931.

Rex, A. J., Searle, M. P., Tirrul, R., Crawford, M.B., Prior, D. J., Rex, D. C. & Barnicoat, A. (1988). The geochemical and tectonic evolution of the Central Karakorum, North Pakistan. *Philosophical Transactions of the Royal Society of London, Series A* **326**, 229–255.

Rolland, Y., Pêcher, A. & Picard, C. (2000). Middle Cretaceous back-arc formation and arc evolution along the Asian margin: the Shyok Suture Zone in northern Ladakh (NW Himalaya). *Tectonophysics* **325**, 145–173.

Rolland, Y., Mahéo, G., Guillot, S. & Pêcher, A. (2001). Tectono-metamorphic evolution of the Karakorum Metamorphic Complex

(Dassu–Askole area, NE Pakistan): exhumation of mid-crustal HT–MP gneisses in a convergent context. *Journal of Metamorphic Geology* **19**, 717–737.

Rolland, Y., Picard, C., Pêcher, A., Carrio, E., Sheppard, S. M. F., Oddone, M. & Villa, I. M. (2002*a*). Presence and geodynamic significance of Cambro-Ordovician series of SE Karakoram (N Pakistan). *Geodinamica Acta* **15**, 1–21.

Rolland, Y., Picard, C., Pêcher, A., Lapierre, H., Bosch, D. & Keller, F. (2002*b*). The Cretaceous Ladakh arc of NW Himalaya—slab melting and melt–mantle interaction during fast northward drift of Indian Plate. *Chemical Geology* **182**, 139–178.

Rowley, D. B. (1996). Age of initiation of collision between India and Asia: a review of stratigraphic data. *Earth and Planetary Science Letters* **145**, 1–13.

Schaltegger, U., Zeilinger, G., Frank, M. & Burg, J. P. (2002). Multiple mantle sources during island arc magmatism: U–Pb and Hf isotopic evidence from the Kohistan arc complex, Pakistan. *Terra Nova* **14**, 461–468.

Schärer, U., Copeland, P., Harrison, T. M. & Searle, M. P. (1990). Age, cooling history and origin of post-collisional leucogranites in the Karakoram Batholith: A multi system isotopic study, N. Pakistan. *Journal of Geology* **98**, 233–251.

Searle, M. P., Rex, A. J., Tirrul, R., Rex, D. C., Barnicoat, A. & Windley, B. F. (1989). Metamorphic, magmatic, and tectonic evolution of the central Karakoram in the Biafo–Baltoro–Hushe regions of northern Pakistan. In: Malinconico, L. L. & Lillie, R. J. (eds) *Tectonics and Geophysics of the Western Himalaya. Geological Society of America, Special Papers* **232**, 47–74.

Searle, M. P., Crawford, M. B. & Rex, A. J. (1992). Field relations, geochemistry, origin and emplacement of the Baltoro granite, Central Karakorum. *Transactions of the Royal Society of Edinburgh: Earth Sciences* **83**, 519–538.

Seghedi, I., Balintoni, I. & Szakacs, A. (1998). Interplay of tectonics and Neogene post-collisional magmatism in the Intracarpathian region. *Lithos* **45**, 483–497.

Sobel, E. R. & Arnaud, N. (2000). Cretaceous–Paleogene basaltic rocks of the Tuyon basin, NW China and the Kyrgyz Tian Shan: the trace of a small plume. *Lithos* **50**, 191–215.

Stern, T., Molnar, P., Okaya, D. & Eberhart-Phillips, D. (2000). Teleseismic P wave delays and modes of shortening the mantle lithosphere beneath South Island, New Zealand. *Journal of Geophysical Research* **105**, 21615–21631.

Tanaka, T., Tamimizu, M., Asahara, Y., Yonezawa, C., Toyashi, S. & Kamioka, M. (1996). A variety of ^{143}Nd/^{144}Nd ratios among six high purity neodymium reagents. *Journal of the Mass Spectrometry Society of Japan* **44**, 79–83.

Tarney, J. & Jones, C. E. (1994). Trace-Element Geochemistry of Orogenic Igneous Rocks and Crustal Growth-Models. *Journal of the Geological Society* **151**, 855–868.

Thompson, A. B. & Connolly, J. A. D. (1995). Melting of the continental crust; some thermal and petrological constraints on anatexis in continental collision zones and other tectonic settings. *Journal of Geophysical Research* **100**, 15565–15579.

Treloar, P. J., Coward, M. P., Williams, M. P. & Khan, M. A. (1989). Basement–cover imbrication south of the Main Mantle Thrust, north Pakistan. In: Malinconico, L. L. & Lillie, R. J. (eds) *Tectonics and Geophysics of the Western Himalaya. Geological Society of America, Special Papers* **232**, 137–152.

Turner, S., Sandiford, M. & Foden, J. (1992). Some geodynamic and compositional constraints on postorogenic magmatism. *Geology* **20**, 931–934.

Turner, S., Arnaud, N., Liu, J., Rogers, N., Hawkesworth, C. N., Harris, S. K., Van Calsteren, P. & Deng, W. (1996). Post-collision, shoshonitic volcanism on the Tibetan Plateau: implications for convective thinning of the lithosphere and source of ocean island basalt. *Journal of Petrology* **37**, 45–71.

Turner, S. P., Platt, J. P., George, R. M. M., Kelley, S. P., Pearson, D. G. & Noveww, G. M. (1999). Magmatism associated with orogenic collapse of the Betic–Alboran domain, SE Spain. *Journal of Petrology* **40**, 1011–1036.

Van der Voo, R., Spakman, W. & Bijwaard, H. (1999). Tethyan subducted slabs under India. *Earth and Planetary Science Letters* **171**, 7–20.

Van de Zedde, D. M. A. & Wortel, M. J. R. (2001). Shallow slab detachment as a transient source of heat at midlithospheric depths. *Tectonics* **20**, 868–882.

Venturelli, G., Capedri, S., Dibattistini, G., Crawford, A., Kogarko, L. N. & Celestini, S. (1984). The ultrapotassic rocks from southeastern Spain. *Lithos* **17**, 37–54.

Vervoort, J., Patchett, P. J., Blichert-Toft, J. & Albarède, F. (1999). Relationships between Lu–Hf and Sm–Nd isotopics systems in the global sedimentary system. *Earth and Planetary Science Letters* **168**, 79–99.

Villa, I. M., Lemennicier, Y. & LeFort, P. (1996). Late Miocene to Early Pliocene tectonometamorphism and cooling in south–central Karakorum and Indus–Tsangpo suture, Chogo Lungma area (NE Pakistan). *Tectonophysics* **260**, 201–214.

Visona, D. & Lombardo, B. (2002). Two-mica and tourmaline leucogranites from the Everest–Makalu region (Nepal–Tibet). Himalayan leucogranite genesis by isobaric heating? *Lithos* **62**, 125–150.

Wang, Q., Wyman, D. A., Xu, J. F., *et al.* (2008). Eocene melting of subducting continental crust and early uplifting of central Tibet: Evidence from central–western Qiangtang high-K calc-alkaline andesites, dacites and rhyolites. *Earth and Planetary Science Letters* **272**, 158–171.

Williams, H., Turner, S., Kelley, S. & Harris, N. (2001). Age and composition of dikes in Southern Tibet: New constraints on the timing of east–west extension and its relationship to postcollisional vocanism. *Geology* **29**, 339–342.

Williams, H. M., Turner, S. P., Pearce, J. A., Kelley, S. P. & Harris, N. B. W. (2004). Nature of the source regions for post-collisional, potassic magmatism in southern and northern Tibet from geochemical variations and inverse trace element modelling. *Journal of Petrology* **45**, 555–607.

Zafar, M., Murata, M., Khan, T., Ozawa, H. & Nishimura, H. (2000). Major and trace element compositions of post-collisional, peraluminous Garam Chashma Granite, Hindukush Range, northwestern Pakistan. *Journal of Mineralogical and Petrological Sciences* **95**, 173–181.

Zafar, M., Murata, M., Ali, A., Jabeen, I., Khan, T., Ozawa, H. & Nishimura, H. (2001). Oxygen isotope compositions of Miocene Garam Chashma granites, Trans-Himalayas (Hindukush Range), North Pakistan. *Journal of Mineralogical and Petrological Sciences* **96**, 197–204.

Zanchi, A. & Gaetani, M. (1994). Introduction to the geological map of the North Karakorum terrain from the Chapursan Valley to the Shimshal Pass 1:150,000 scale. *Rivista Italiana di Paleontologia e Stratigrafia* **100**, 125–135.

Zhang, L. S. & Schärer, U. (1999). Age and origin of magmatism along the Cenozoic Red River shear belt, China. *Contributions to Mineralogy and Petrology* **134**, 67–85.

Zhou, H. W. & Murphy, M. A. (2005). Tornographic evidence for wholesale underthrusting of India beneath the entire Tibetan plateau. *Journal of Asian Earth Sciences* **25**, 445–457.

Zindler, A. & Hart, S. (1986). Chemical geodynamics. *Annual Review of Earth and Planetary Sciences* **14**, 493–571.